ORNL/TM-2012/174

OAK RIDGE
NATIONAL LABORATORY
MANAGED BY UT-BATTELLE
FOR THE DEPARTMENT OF ENERGY

Advanced High-Temperature Reactor Dynamic System Model Development

April 2012 Status

Rev 0
April 30, 2012

Prepared by

A. L. Qualls
M. S. Cetiner
T. L. Wilson Jr.

UT-BATTELLE
ORNL-27 (4-00)

ORNL/TM-2012/174

Reactor and Nuclear Systems Division

ADVANCED HIGH-TEMPERATURE REACTOR DYNAMIC SYSTEM MODEL DEVELOPMENT

APRIL 2012 STATUS

A. L. Qualls
M. S. Cetiner
T. L. Wilson Jr.

April 2012

Prepared by
OAK RIDGE NATIONAL LABORATORY
Oak Ridge, Tennessee 37831-6283
managed by
UT-BATTELLE, LLC
for the
U.S. DEPARTMENT OF ENERGY
under contract DE-AC05-00OR22725

CONTENTS

Page

LIST OF FIGURES

LIST OF TABLES

ACRONYMS

AHTR	Advanced High-Temperature Reactor
AWTS	Accident without Scram
BLT	Block Lower Triangular
DAE	differential-algebraic equation
DRACS	Direct Reactor Auxiliary Cooling System
FHR	Fluoride-Salt-Cooled High-Temperature Reactor
HPT	high-pressure turbine
LOFF	loss of forced flow
LOOP	loss of offsite power
LWR	Light Water Reactor
ODE	ordinary differential equation
PCS	Power Conversion System
PHTS	Primary Heat Transport System
P-IHX	primary-to-intermediate heat exchangers
RCB	Reactor Containment Building
RVACS	Reactor Vessel Auxiliary Cooling System
SHTS	Secondary Heat Transport System
UHS	Ultimate Heat Sink

1. INTRODUCTION

The Advanced High-Temperature Reactor (AHTR) is a large-output fluoride-salt-cooled high-temperature reactor (FHR). An early-phase preconceptual design of a 1500 MW(e) power plant was developed in 2011 [Refs. 1 and 2]. An updated version of this plant is shown as Fig. 1. FHRs feature low-pressure liquid fluoride salt cooling, coated-particle fuel, a high-temperature power cycle, and fully passive decay heat rejection. The AHTR is designed to be a "walk away" reactor that requires no action to prevent large off-site releases following even severe reactor accidents. This report describes the development of dynamic system models used to further the AHTR design toward that goal. These models predict system response during warmup, startup, normal operation, and limited off-normal operating conditions. Severe accidents that include a loss-of-fluid inventory are not currently modeled.

The scope of the models is limited to the plant power system, including the reactor, the primary and intermediate heat transport systems, the power conversion system, and safety-related or auxiliary heat removal systems. The primary coolant system, the intermediate heat transport system and the reactor building structure surrounding them are shown in Fig. 2. These systems are modeled in the most detail because the passive interaction of the primary system with the surrounding structure and heat removal systems, and ultimately the environment, protects the reactor fuel and the vessel from damage during severe reactor transients. The reactor silo also plays an important role during system warmup.

The dynamic system modeling tools predict system performance and response. The goal is to accurately predict temperatures and pressures within the primary, intermediate, and power conversion systems and to study the impacts of design changes on those responses. The models are design tools and are not intended to be used in reactor qualification. The important details to capture in the primary system relate to flows within the reactor vessel during severe events and the resulting temperature profiles (temperature and duration) for major components. Critical components include the fuel, reactor vessel, primary piping, and the primary-to-intermediate heat exchangers (P-IHXs). The major AHTR power system loops are shown in Fig. 3. The intermediate heat transfer system is a group of three pumped salt loops that transports the energy produced in the primary system to the power conversion system.

Two dynamic system models are used to analyze the AHTR. A Matlab/Simulink®-based model initiated in 2011 has been updated to reflect the evolving design parameters related to the heat flows associated with the reactor vessel. The Matlab model utilizes simplified flow assumptions within the vessel and incorporates an empirical representation of the Direct Reactor Auxiliary Cooling System (DRACS). A Dymola/Modelica® model incorporates a more sophisticated representation of primary coolant flow and a physics-based representation of the three-loop DRACS thermal hydraulics. This model is not currently operating in a fully integrated mode. The Matlab model serves as a prototype and provides verification for the Dymola model, and its use will be phased out as the Dymola model nears completion. The heat exchangers in the system are sized using spreadsheet-based, steady-state calculations. The detail features of the heat exchangers are programmed into the dynamic models, and the overall dimensions are used to generate realistic plant designs. For the modeling cases where the emphasis is on understanding responses within the intermediate and primary systems, the power conversion system may be modeled as a simple boundary condition at the intermediate-to-power conversion system heat exchangers.

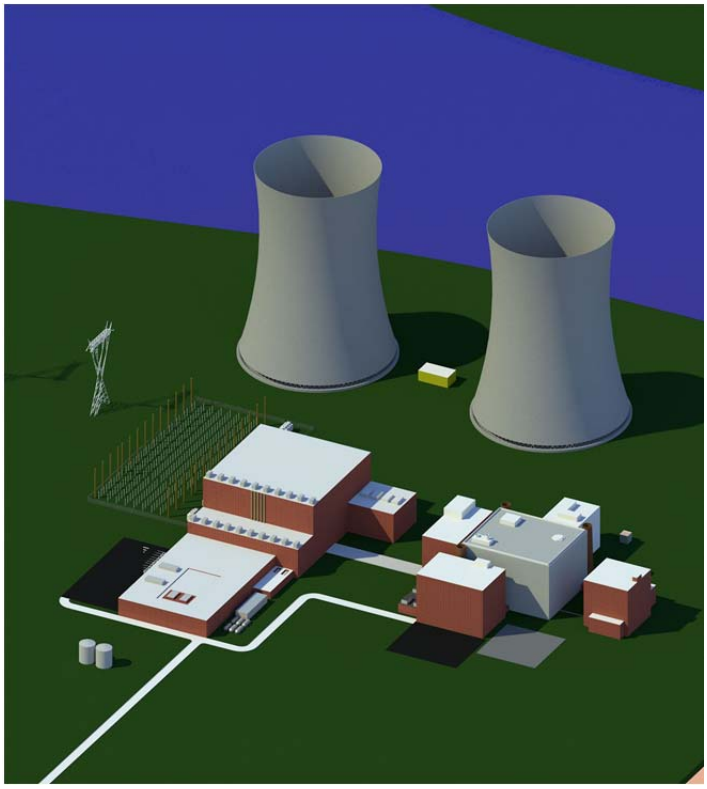

Fig. 1. The AHTR central generation station utilizing hybrid cooling for waste heat rejection.

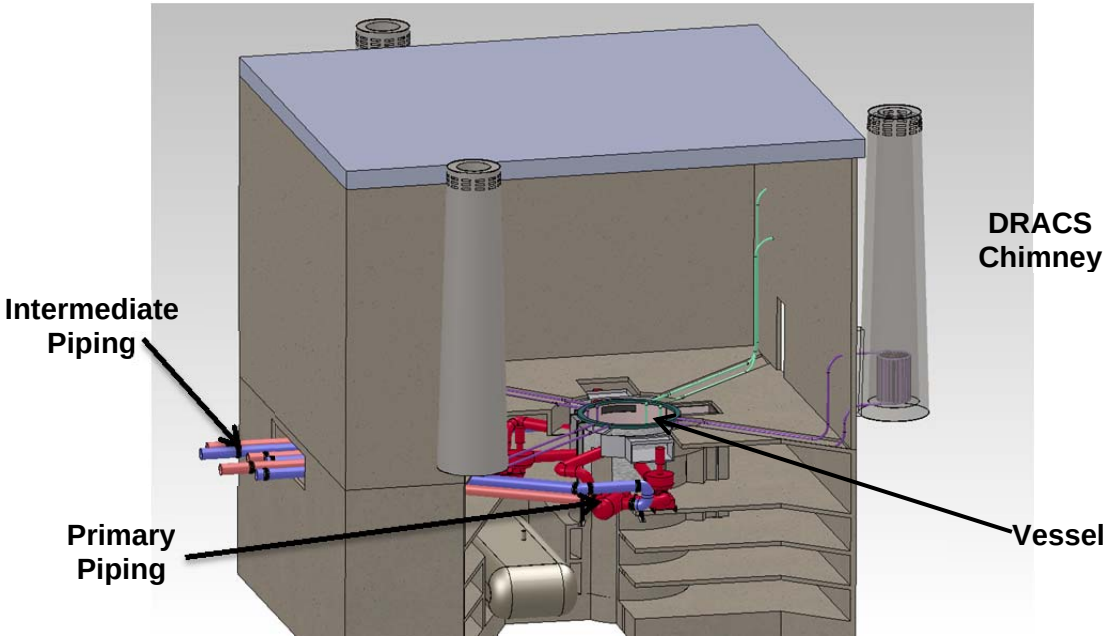

Fig. 2. Rendering of the AHTR primary system and reactor building.

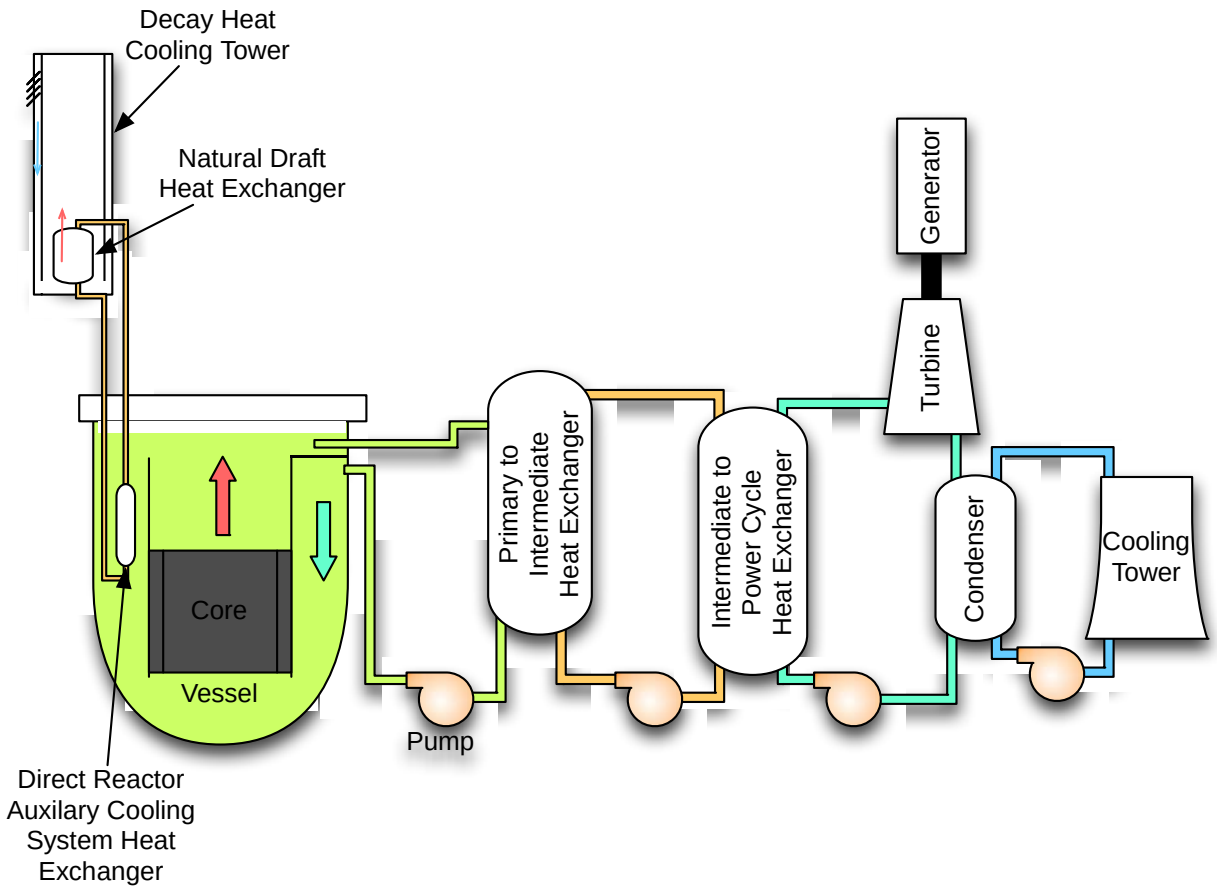

Fig. 3. The AHTR power system loops.

The nominal power performance parameters of the AHTR are listed in Table 1 [Ref. 3].

Table 1. Nominal power performance parameters of the AHTR

Parameter	Unit	Value
Reactor thermal power	MW	3400
Electrical power	MW	1531.4
Net thermal efficiency	%	45.0
Primary coolant		$2^{7}LiF\text{-}BeF_2$
Lithium-7 enrichment level	%	99.995
Intermediate coolant	mole %	$KF\text{-}ZrF_4$ (47–53)
Power cycle fluid		Water
Fuel type		UCO coated particle
Uranium-235 enrichment level	%	9
Core power density	MW/m^3	12.9
Reflector material		Graphite
Reactor vessel internals material		SiC-SiC composite
Core structural material		C-C composite
Control blade material		MoHfC alloy
Primary coolant flow rate	kg/s	28,500
Number of primary loops		3
Number of intermediate loops		3
Number of power cycle loops		2
Refueling interval	Months	6
Refueling outage duration	Days	2
Fuel format		Plates in hexagonal grid
Mixed mean core outlet temperature	°C	700
Core inlet temperature	°C	650
Number of plates per assembly		18
Number of fuel assemblies		252
Maximum fuel temperature (average assembly)	°C	854
Average coolant velocity along fuel	m/s	1.93
Vessel material		Alloy 800H
Liner material		Alloy N
Core fueled height	m	5.5
Core pressure drop for normal operation	atm	1

2. AHTR DESIGN RELATED TO PERFORMANCE

The AHTR dynamic models are limited to reactor fuel, core, primary and intermediate salt-based heat transport systems, and the power conversion systems. Only those systems that can influence the reactor power or the temperatures and pressures within these systems are modeled. In the case of the reactor primary system, the vessel can lose heat to the surrounding structure of the reactor building. In the case of the intermediate system, the long transport piping can lose heat to the tunnel enclosure that extends between the reactor building and the power conversion building.

2.1 PRIMARY COOLANT SYSTEM

The AHTR primary system is a blend of a pool and a loop design. Heat is generated by the reactor core, which is located within a pool of primary coolant normally under forced flow. The nominal thermal power in the AHTR is 3400 MW(t). The mixed mean reactor coolant outlet temperature is 700°C. $2^{7}LiF$-BeF_2 (enriched in ^{7}Li to 99.995%), referred to as FLiBe, is the primary coolant. A 53% KF 47% ZrF_4 (mole %) fluoride salt mixture was chosen for the intermediate loop as a compromise among heat transfer performance, melting temperature, and cost. KF-ZrF_4 was also chosen for the DRACS because of the same criteria and the desire to limit the number of salt compositions used. While FLiBe is a reasonably well-known fluoride salt coolant, even the melt point of KF-ZrF_4 is uncertain, with a 40°C discrepancy (390°C vs 430°C) between the two published phase diagrams.[4] Thus, the parameters for KF-ZrF_4 quoted are preliminary, and additional certainty in coolant parameters is required.

The core produces 3400 MW(t) of fission power within 252 fuel assemblies, as shown in Fig. 4. The upper temperature limit of 700°C arises from the decrease in strength with increasing temperature of Alloy 800H and Alloy N,[5] which are the near-term structural alloys selected for the reactor vessel and primary piping. Operational events result in temperature responses within the primary system structural materials. Understanding these responses and how system design affects them is the purpose of the dynamic system model development effort. Transient responses directly relate to the allowable operating envelope of the plant and ultimately determine how it must be controlled and how efficiently it can operate.

The temperature increase across the core is held by design to 50°C, and a primary coolant flow rate of 28,500 kg/s is required to maintain the 50°C temperature increase across the core at full power. The primary coolant enters the reactor vessel through three segmented downcomer sections that direct the cold-leg coolant downward to the lower plenum. The coolant flows upward from the lower plenum to cool the fuel assemblies. The fuel assemblies are composed of 18 fuel planks suspended from a central “Y”-shaped support structure, as shown in Figs. 5 and 6.

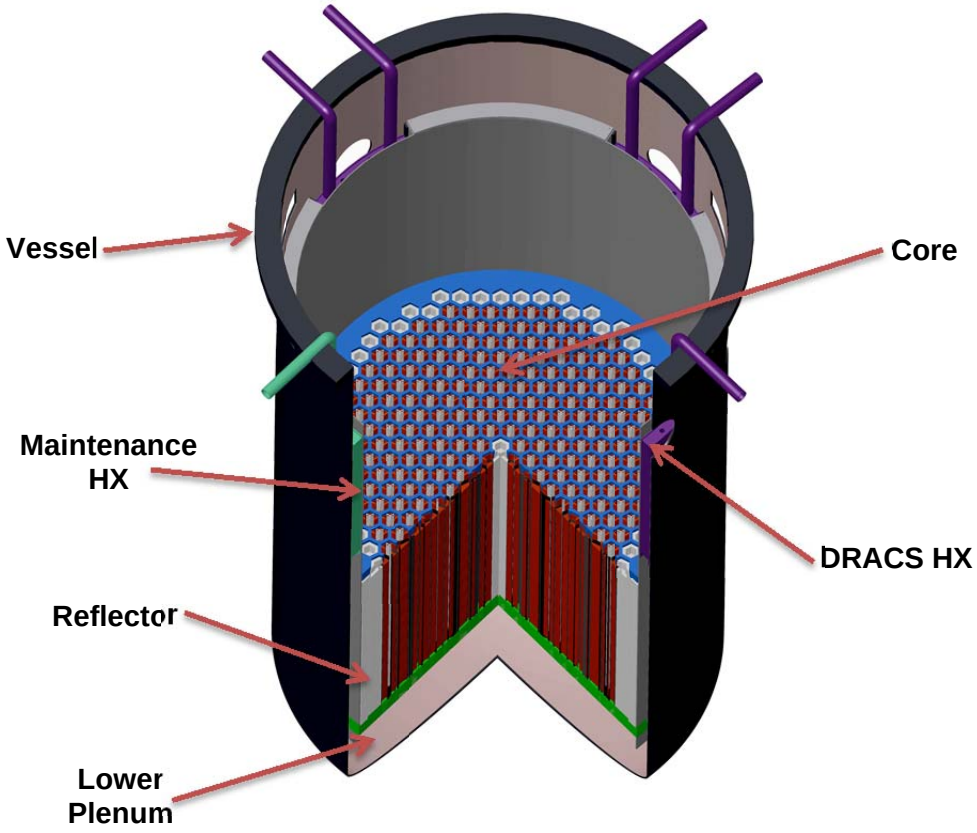

Fig. 4. Cutaway view of the AHTR core and vessel.

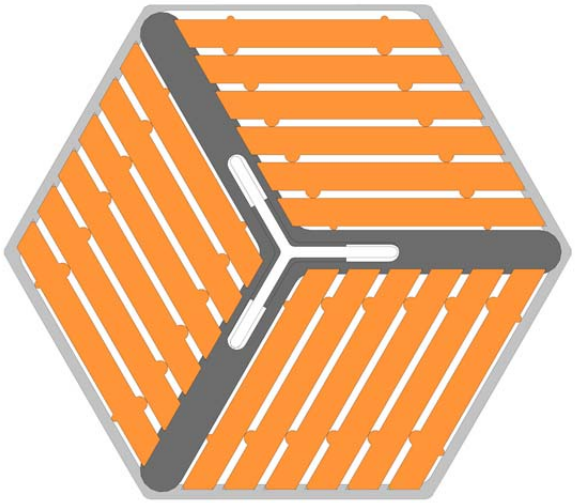

Fig. 5. Top view of an AHTR fuel bundle containing 18 fuel elements.

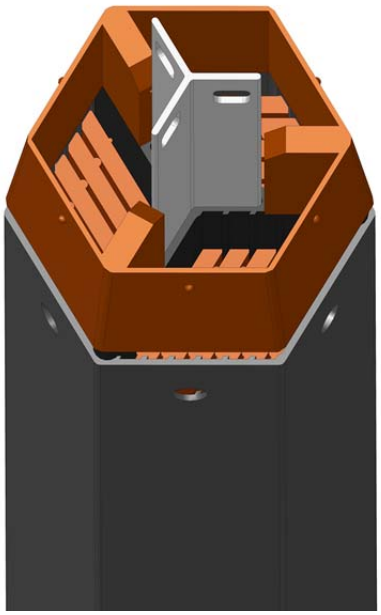

Fig. 6. View of an AHTR fuel bundle and supporting structure. Eighteen fuel plates are hung from the support "Y," and the entire assembly is surrounded by a fuel channel box.

Each inner fuel plank is cooled by two ~24 cm by 0.7 cm interior coolant channels, and the outer planks are cooled by one interior channel and an outer channel with approximately half the thickness and coolant flow. Only half of the heat generated in an outer plank enters the thinner channels; thereby, the coolant experiences approximately the same temperature increase as that in the inner channels. The major flow paths within the reactor vessel are shown in Fig. 7.

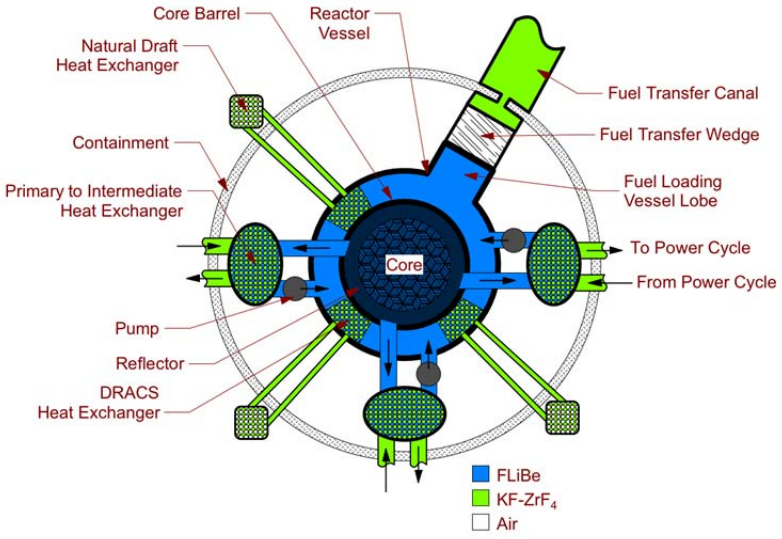

Fig. 7. Schematic showing the flow patterns of the AHTR reactor system including the P-IHX and the DRACS.

The primary coolant flow rate is split evenly over three primary coolant legs, and the velocity in the connecting primary system piping is limited by design to 4 m/s. The inner diameter (ID) required for maintaining the flow velocity is approximately 1.24 m. The reactor pressure vessel has three primary outlet pipes and three return pipes. These six ports are positioned on the perimeter of the cylindrical portion of the reactor vessel in an upper plenum below the top flange.

Three primary-to-intermediate loop salt-to-salt heat exchangers (P-IHX) transfer heat from the primary system to the intermediate system. These heat exchangers are located near the reactor vessel within the primary containment structure, and each heat exchanger handles one-third of the primary coolant flow and transfers one-third of the thermal power to the intermediate salt heat transfer system.

After exiting the vessel, the primary coolant enters the P-IHXs and flows through it to the P-IHX outlets, where electrically driven pumps force it back to the vessel. The primary coolant enters the vessel at the same level as the outlet piping and flows into downcomer channels that direct the flow downward along the reactor vessel wall. This arrangement allows the vessel wall to operate near the lowest primary coolant temperature—650°C. Flow from the downcomers enters a lower plenum and reverses direction to flow up through the core. The lower core support structure contains orifices to distribute flow to the channels within individual fuel assemblies.

The flow will be limited in radial sectors of the core based on detailed thermal hydraulic analyses that are to be completed in 2013. The dynamic system models use simplified representations of flow through the vessel and core. The objective of the simplified models is to accurately represent the flow with minimal computational effort on flexible and transportable platform. In the Dymola/Modelica models, the flows are modeled in distinctive loops with separate flows. In the Matlab/Simulink model, a single flow channel is used to model the three primary loops' flows, and it is assumed they behave identically.

The reactor core is modeled in four radial sections, each with selectable power densities. The outer channel represents a radial reflector which has a low volumetric power density. The three remaining radial sectors thermal power densities generally peak in the central stack and progressively decrease in middle and outer rings surrounding the central stack. Axial power profiles are programmed into the radial sections so that the core is modeled with both a radial and axial power profile.

The salt coolants have melting temperatures greater than ambient temperature; therefore, the reactor primary and intermediate loops must be heated prior to the initial loading of the fluids. The systems must also remain above the salt melting temperatures whenever it is filled with salt. A notional heating arrangement for the vessel is shown in Fig. 8, and views of the gap design between the vessel and the reactor silo concrete is shown in Fig. 9.

Heat is lost from the vessel to the surrounding reactor building structure across the following gaps and structures.

1. Vessel wall
2. Inner argon-filled gap
3. Insulation and heated enclosure
    a. Inner heated wall with electrical cartridge heaters facing the vessel
    b. Insulation-filled wall
    c. Outer insulation backing and shield wall
4. Outer argon-filled gap
5. Stainless steel liner
6. Concrete

The temperature of the concrete must be maintained at temperatures low enough to prevent degradation over the lifetime of the plant. A cooling system is employed to maintain the required temperature levels, and the dynamic system models will be used to determine the performance requirements of the system.

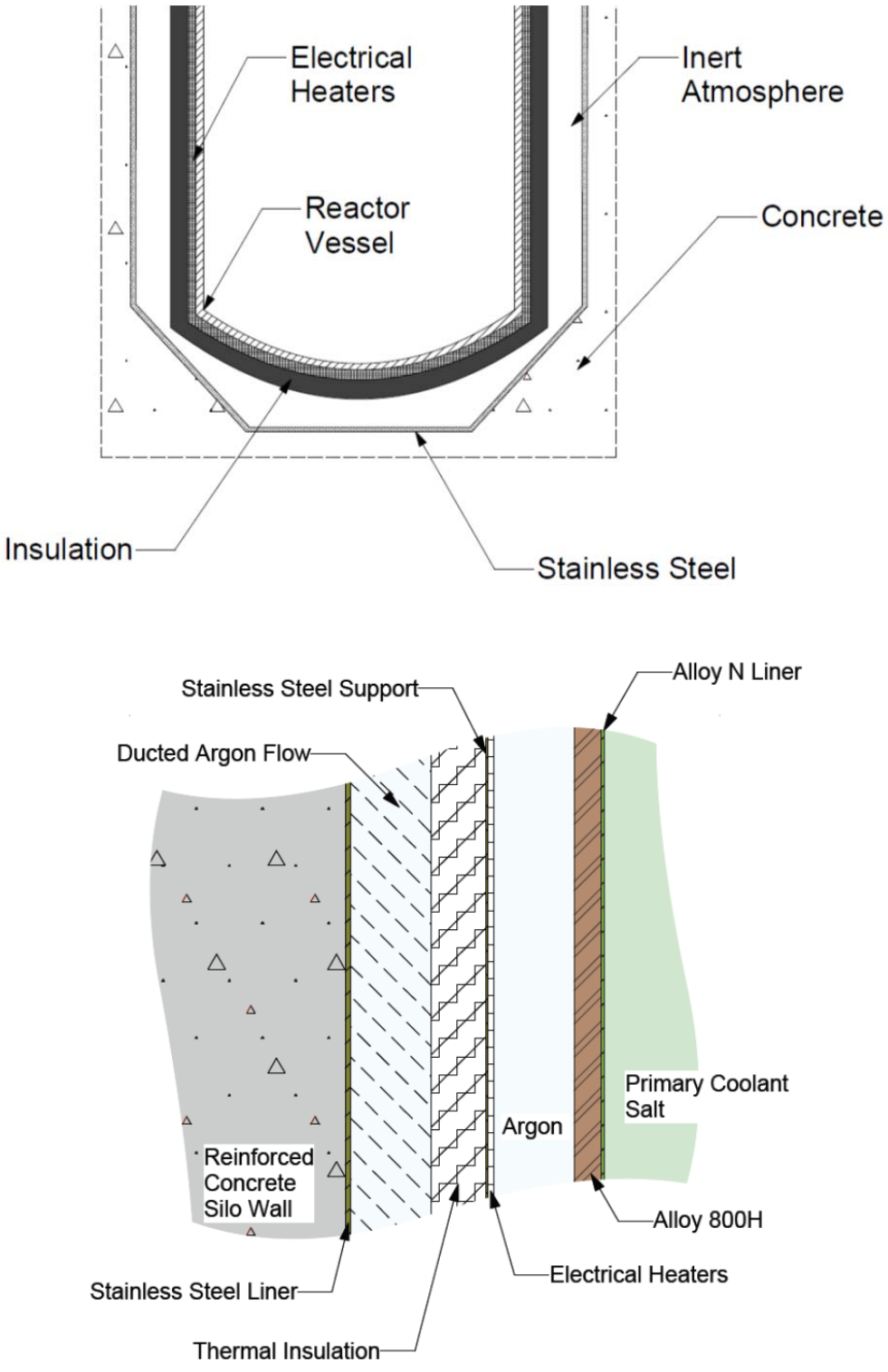

Fig. 8. Notional arrangement of the reactor vessel within a reactor cavity. The vessel is encased in heaters and insulation and is isolated from the concrete with a dry inert gas-filled gap. The melting point of the primary coolant is 459°C.

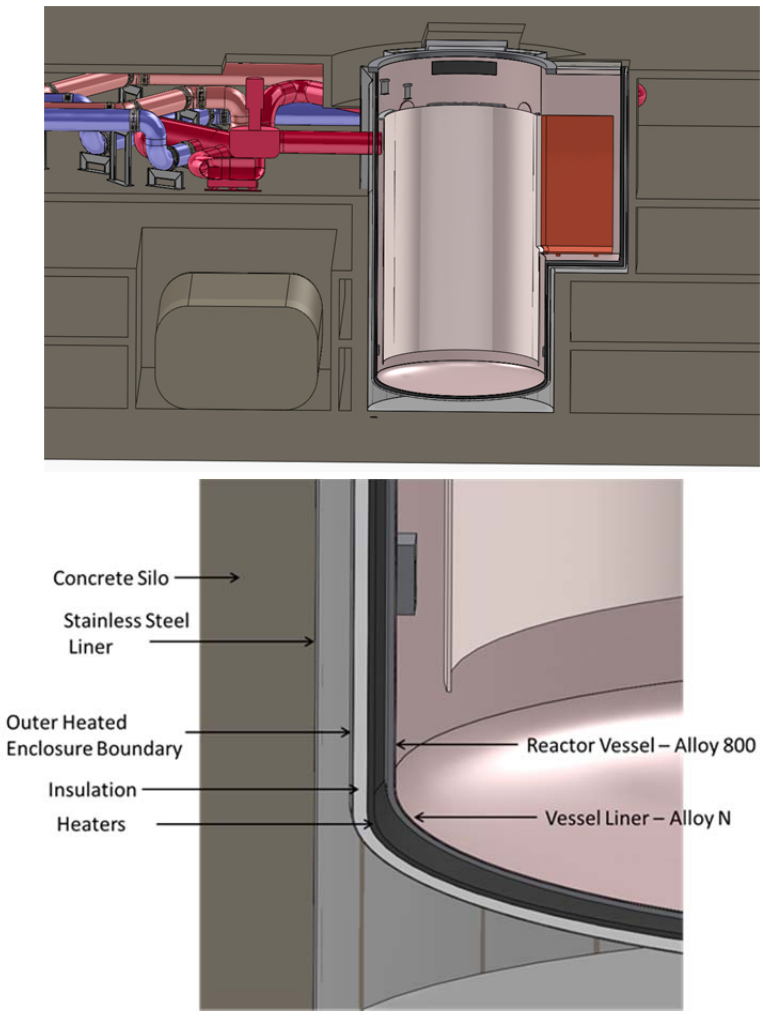

Fig. 9. Detail of the region between the reactor vessel and the reactor silo concrete surrounding.

2.2 PASSIVE SAFETY

FHRs have substantially larger negative reactivity thermal feedback than LWRs due primarily to their coated particle fuel. The AHTR's negative temperature feedback coefficient of reactivity causes the reactor power to decrease as temperatures increase during an accident scenario (even in the absence of other control action). This passive safety feature is the first line of defense against reactor core and vessel damage. Actively inserted control blades are the next line of defense against overpower accidents. The control blades are held up out of the core with fusible links. These links are designed to melt in the event that the primary coolant increases to a level (to be determined) above the nominal operating temperature. Specific alloys and melt points have not yet been selected.

A neutron-absorbing salt injection system with provision for both passive and active operation is included on the AHTR as a secondary reactor shutdown system. Currently, this system is envisioned as a series of canisters sealed with a gold-tin braze alloy set to melt at a temperature above the melt temperature of the control blade release links. As the temperature of the primary salt increases above the melt point of the braze, the canisters open to release salts containing neutron-absorbing isotopes into the primary coolant in the lower plenum. This will pull neutron poison into the core and shut down the fission

chain reaction. It is highly desirable to limit system thermal response during normally anticipated transients so that the control blade fusible links do not melt and the poison salt is not released. Current analyses do not include the activation of these systems so that temperature excursions in the absence of reactor scram can be studied.

The AHTR utilizes a low-pressure coolant with a high boiling point (1400°C) and high-temperature fuel. The system is also large and has high heat capacitance. Thus, the time between the initiation of an accident scenario and the approach to damage is expected to be longer for the AHTR compared to light water reactors. Thus, responses can occur less suddenly, which opens up the possibility that passive safety systems may be adequate to avoid fuel or vessel damage.

The three auxiliary means of removing heat from the primary system are (1) by allowing it to flow through and out of the reactor primary vessel to surrounding structure, (2) by direct cooling of the primary system with the DRACS, and (3) by the use of a forced-flow heat exchanger in direct contact with the primary coolant. The forced-flow heat exchanger is planned for use during regular maintenance outages but it could be used during off-normal operations. Of these systems, only the DRACS is considered to be a safety-related system.

2.2.1 Direct Reactor Auxiliary Cooling System

The DRACS pulls heat from the reactor primary coolant and dissipates it to the atmosphere via three independent, three-loop natural circulation systems, as shown schematically in Figs. 10 and 11. The primary coolant is the first fluid in the three-loop system. The coolant temperature rise due to the core decay heat provides the buoyancy force for primary coolant flow upward through the core upon loss of forced flow. The DRACS heat exchangers remove the heat and are located near the top of the downcomer to maximize gravity-driven natural circulation down the vessel downcomer and upward through the core.

The second DRACS loop is an enclosed salt loop transferring heat from the DRACS in-vessel salt-to-salt heat exchanger to a natural draft salt-to-air heat exchanger outside the containment. Thus, the DRACS heat exchangers are filled with KF-ZrF_4, and the primary salt and the air flow over the outside of vertical piping enclosing the fluid in the heat exchangers.

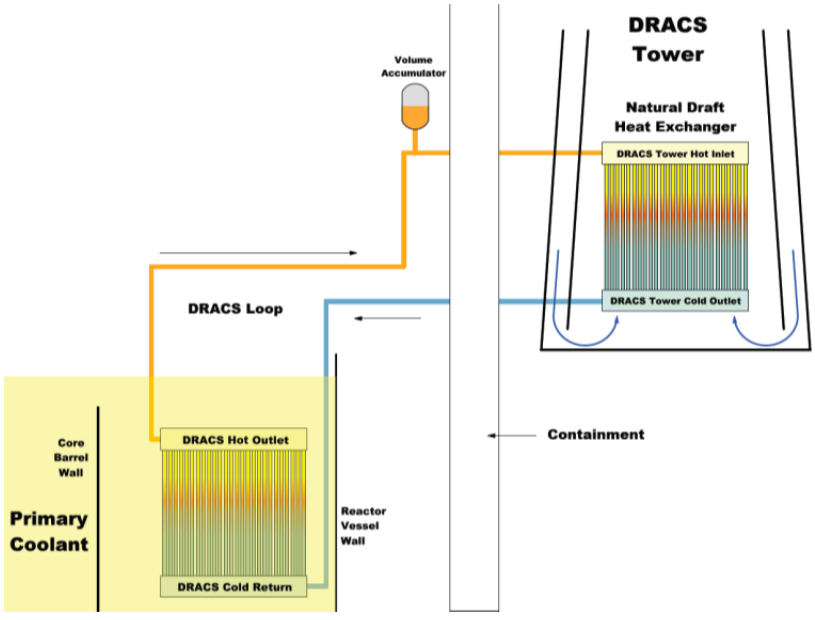

Fig. 10. Two of the three salt-to-salt DRACS heat exchangers.

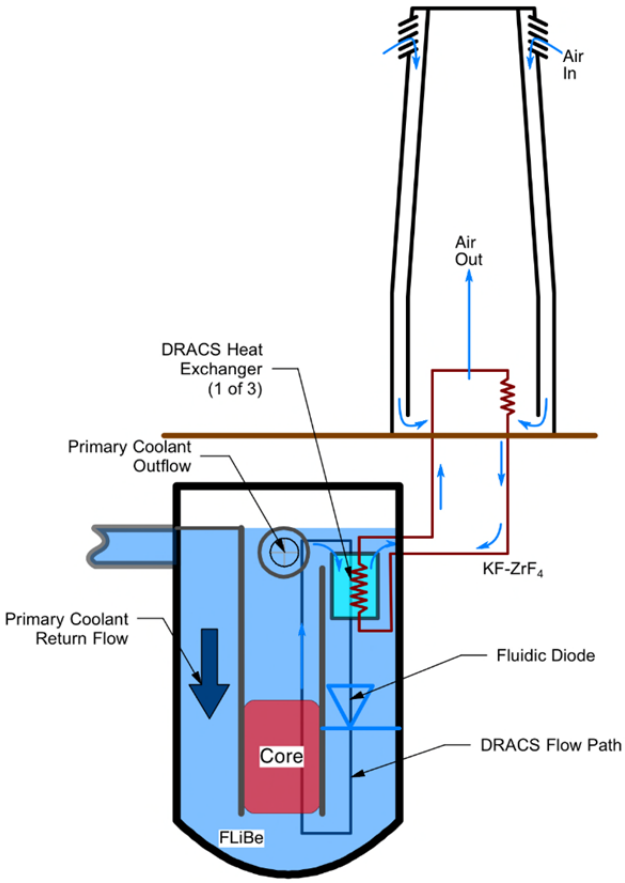

Fig. 11. Diagram of the reactor primary coolant arrangement within the vessel and the DRACS.

Air is the third fluid in the DRACS and the ultimate heat sink. The DRACS intermediate heat transfer system piping requires penetrations through the reactor containment structure to allow the salt-to-air heat exchanger to be located outside. The diameter, number of bends, and overall length of this piping is important in determining performance. The elevation difference between the DRACS heat exchangers is also an important determinant of performance.

The design of the DRACS heat exchangers is ongoing. The loops are sized so that two of the three loops will prevent damage to reactor components following major accident scenarios. The current design assumes that each DRACS can pull out 0.25% of full reactor power at 700°C mixed-mean coolant temperature under fully established natural circulation flow after a loss-of-forced-flow accident. This assumption sets the steady-state heat rejection requirement of each DRACS at 8.5 MW.

During normal operation, 650°C primary coolant flows in the reverse direction (upward) at a reduced rate over the DRACS in-vessel heat exchangers. Fluidic diodes below the DRACS heat exchangers limit the amount of coolant flow that can flow upward over the heat exchangers during normal operation so that the majority of the primary coolant flow passes upward through the core. If the primary pumps lose power and coast down to a full stop, the pressure distribution within the core changes due to buoyancy effects. Heat from the core causes warmer coolant to rise to the upper plenum and flow through the fluidic diodes eventually stop, reverse, and increase. This pulls warmer coolant from the upper plenum downward over the DRACS heat exchangers where it is cooled. The size and the spacing of the heat exchanger tubes determine the flow resistance of the primary coolant past the heat exchanger and its heat transfer characteristics.

The heated salt within the DRACS heat exchanger begins to rise and flow outside the containment building where it passes through the air-to-salt heat exchanger and is cooled by the natural updraft of air within a natural circulation cooling tower. The design of this heat exchanger, like the salt-to-salt heat exchanger, is a trade between flow restriction and heat transfer coefficient.

Normal DRACS bypass flow maintains the intermediate DRACS salt loop in a liquid state without the need for electrical heaters, although the system is fully electrically heated to prevent freezing when the reactor is not operating. The DRACS is, therefore, operational under normal operating conditions, and the plant suffers a modest performance loss for having the safety feature in hot standby. Louvers on the DRACS chimney are actively closed to minimize heat loss during system warmup and normal operation. The louvers are the only active portion of the DRACS system. In the event of a loss of power to the site, the louvers open automatically. As the core temperature initially increases during a loss-of-forced-flow accident, the flow rates in the DRACS loops increase (and reverse in the case of the downcomer flow) until a new heat loss and production equilibrium is established. The flow rates and heat loss gradually decrease as the decay heat in the core decreases.

The transient response of reactor core flow due to the loss of primary pump power proceeds as follows.

1. Pressure at the reactor vessel inlet is reduced as the primary pumps coast down, resulting in reduced flow through the core.
2. Temperature increases within the core, causing the reactor power to decrease and increased natural circulation forces in the core due to volumetric expansion of the coolant.
3. The pressure difference across the fluidic diodes reverses; upward flow through the DRACS in-vessel HXs stops and then reverses.
4. A natural circulation pattern within the core is established with upward flow through the reactor core and downward flow over the DRACS heat exchangers through the fluidic diodes (in the low flow resistance direction) and into the lower plenum.
5. The DRACS removes heat from the primary coolant, heating the fluid within the DRACS heat exchangers, and increasing the natural circulation driving potential of the DRACS secondary flow loop.

Placing both the inlet and outlet piping above the core allows siphon breaks in the piping to prevent the loss of enough coolant from the vessel to uncover the core or the DRACS heat exchangers in the event of an ex-vessel primary system leak. If a P-IHX were to leak at a low point, when enough coolant is drained to uncover the primary inlet ports, the siphon will be broken and the vessel will contain an enclosed pool of coolant that will still cover the core and the DRACS heat exchangers. Sufficient primary salt is provided in the reactor vessel so that if the vessel were to fail, the primary salt would be contained in the surrounding silo structure contained within the stainless steel liner shown in Fig. 9 in an arrangement that keeps the DRACS heat exchanger covered with salt.

If the reactor fission power is actively shut down in the initial moments of a loss-of-forced-flow transient, any fuel temperature rise will be limited and of short duration. If no control action were to be taken, the fission power will inherently decrease as core temperatures increase. Eventually, equilibrium between a low level of fission power and passive heat removal would be attained, but before this would happen, the fusible links in the control drive mechanisms would melt and drop in the control blades and the secondary, passive melt-point driven poison salt-based shutdown system will activate and mitigate the over-temperature transient. Accident Without Scram (AWTS) events are modeled with the dynamic system models as worst-case scenarios but do not appear to be credible, as they would require the failure of three independent and diverse shutdown mechanisms.

The reactor vessel is sectioned angularly around the perimeter into eight areas. Three areas are where the primary coolant enters the vessel and is directed downward by downcomers to a lower vessel plenum.

Sections containing the DRACS HX and the fluidic diodes are located adjacent to the inlets sections, as shown in Fig. 12. One perimeter section looks similar to a DRACS section; however, the heat exchanger within that section is connected to a forced flow coolant loop. This section is used during maintenance periods and is not included in the dynamic system models. The eighth section is an open section that is used to move fuel into and out of the vessel. The secondary shutdown salt canisters are housed in this area.

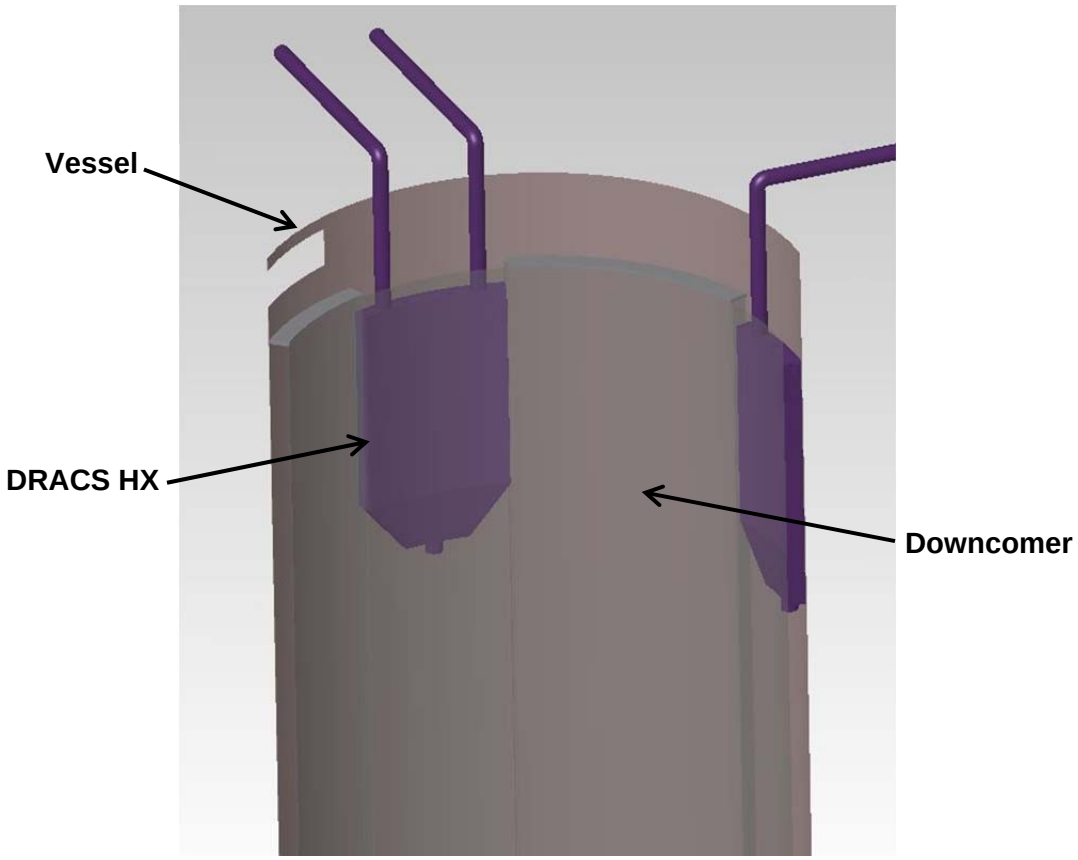

Fig. 12. DRACS salt-to-salt heat exchangers shown within their flow channel at the reactor vessel perimeter.

Flows from eight radial sectors are connected to the reactor vessel lower and upper plenums. The three inlet zones feed the lower plenum and the majority of flow passes through the reactor core to cool the fuel. Upward bypass flow is regulated and limited by the fluidic diodes in the three DRACS sectors. The fuel-handling sector is open as opposed to the other enclosed sectors.

The reactor core barrel surrounds the core and the core reflector sections. Bypass flow passes up along the barrel and receives limited heating. The same is true in the reflector coolant channels. The bypass flows mix within the upper plenum with the heated coolant and reduce the overall temperature within the upper plenum.

Flow within the three primary legs is independent, with each leg having its own P-IHX and electrically powered pump. The primary coolant cools the reactor vessel within the inlet sectors and, to a lesser degree, in those sectors with upward flow from the lower plenum through the fluidic diodes. The flow rates within the three intermediate legs are also independently controlled, but the temperature of the intermediate salt entering the intermediate side of the P-IHXs is equal because the cold legs of the intermediate loops are fed by a common manifold.

The most severe accident scenarios are related to the loss of flow in the primary loops. In the event that all three pumps fail (due to the loss of site electrical power), the flows within the reactor vessel will reestablish to natural circulation conditions which are determined by the DRACS configuration. A significant portion of the modeling effort has been related to representing these flows as they transition from forced flow to natural circulation. Within the sectors with fluidic diodes, the flow will slow and reverse, causing it to temporarily pass through zero velocity. The solutions of the differential equations representing flow experience singularities as the velocity approaches zero and the model can fail. Deliberate solution techniques are being developed to allow solutions to progress through flow reversal situations over a broad range of design space. The solution method of the Dymola software is discussed in Appendix A.

The performance of a DRACS loop is dependent on the following factors.

1. Salt used in the DRACS loop
2. Salt-to-salt heat exchanger design
    a. Number, pitch, inner diameter, wall thickness, material
    b. Tube length
3. Piping connecting DRACS heat exchanger to the salt-to-air heat exchanger
    a. Diameter, wall thickness, material
    b. Lengths, number of bends
    c. Insulation
    d. Elevation differences between the heat exchangers
4. Air-to-salt heat exchanger design
    a. Number, pitch, inner diameter, wall thickness, material
    b. Tube length
5. Air chimney design

To enhance natural circulation, the salt-to-salt and the salt side of the air-to-salt heat exchangers are constructed with upper and lower manifolds separated by vertical piping runs. In the salt-to-salt heat exchanger, the cold DRACS salt returns to the lower manifold and flows upward to the upper manifold. This arrangement makes the heat exchanger a counterflow heat exchanger after flow reversal. During normal operation, the primary coolant flows upward over the heat exchanger in a parallel-flow heat exchanger arrangement. The hot DRACS salt enters the upper manifold of the air-to-salt heat exchanger and flows downward to the lower manifold. Air flows up through the chimney and cools the salt in a counterflow arrangement.

Piping size and layout in the heat exchangers determine pressure drops and heat transfer characteristics. The velocity of the salt in the vertical piping of the heat exchangers must be balanced to increase the heat transfer coefficients while decreasing flow resistance. Spacing of the vertical tubes requires the same trade for the primary salt flowing over the salt-to-salt heat exchanger and the air flowing over the air-to-salt heat exchanger.

During normal operation, the fluidic diode limits the flow of primary salt over the salt-to-salt heat exchanger. This leg of the primary coolant loop is low flow and in a parallel-flow arrangement, thus heat transfer is low. The temperature difference between the salt in the air-to-salt heat exchanger and the salt-to-salt heat exchanger will drive flow in the DRACs salt in the correct direction at a reduced rate. The flow continuously removes heat from the primary salt and induces natural circulation of the air in the DRACS chimneys. Therefore, the air and the DRACS salt circulate in the proper direction, at reduced rates during normal operation. Air inlet louvers are closed to limit air flow and thermal loses. Flow through the DRACS channel in the vessel is reduced and opposite that in the fully developed natural circulation flow. The flow velocities change from these reduced values (and reversed flow in the case of the primary salt) to the fully developed flow velocities of passive response. The performance of the DRACS loops is dependent on the heat produced within the core and the operating characteristics of the

fluidic diodes. Capturing the transient evolution of the DRAC system performance is an essential part of the dynamic system model.

The DRACS system is sized using a worksheet-based calculation that iteratively solves for the steady state temperatures and heat flows under natural circulation within the coupled three-loop system. The thermo-physical properties of the fluids and the physical arrangement and location, particularly elevation, of the heat exchangers are varied to understand how the design variables impact performance. This tool evaluates normal operating conditions (reduced flow, reverse primary flow) and fully developed flow assuming 0.75% of nominal reactor power. The velocities of the air, DRACS salt and the primary salt within the DRACS channel, and the total heat removed are calculated for each design condition. The sizing data is then factored into the dynamic model of the DRACS system.

The object of this calculation is to solve for the flows and temperatures in these three loops given the geometric parameters of the system and the decay heat power. The heat transfer and fluid flow equations can be reduced to formulations in terms of just the hot and cold temperatures in each loop. Ambient temperature is given; thus, five temperatures and three flows are the unknowns in the calculation. The equations that are used to solve for these variables are the energy balances and momentum balances at steady state. The steady-state case simplifies the energy and momentum balances so that they can be solved in a spreadsheet calculation. The calculation makes several other simplifying assumptions. For example, pipes and the reactor vessel wall are assumed adiabatic. The flow is assumed to be laminar (this assumption may be removed by the addition of turbulent heat transfer and friction loss correlations). Symmetric operation of all operating loops is assumed. The number of operational loops can be varied, but no partial operation of a DRACS loop is permitted. The flow in a DRACS loop is either equal to all others or is zero. The bypass channels, which are essentially unheated in decay heat operation, are assumed to have no flow. Flow to the primary heat exchangers is also assumed to be zero.

To facilitate usage as an engineering design tool, the user inputs to the code are just the geometrical parameters of the system. These parameters can be varied to see their impact on temperature and flow under natural circulation conditions. The calculation is designed so that the user enters the minimum set of parameters needed to specify the geometry. The values are propagated throughout the spreadsheet wherever they are needed to update the calculation. Pipes definition requires diameter, length elevation change, and number of bends. Core and heat exchangers involve more complex geometrical inputs, but the principle is the same. The geometry is reduced to a few independent user-input parameters, and the remainder of the calculation is automated.

Material property routines for the coolant salts (FLiBe and KF-ZrF_4), and air are programmed into the spreadsheet to compute viscosity, density, and thermal conductivity as a functions of the temperature. Correlations for heat transfer in free convection regime and Darcy friction factor are built into the calculation to evaluate the necessary variables for the flow and energy equations.

The spreadsheet calculation is divided into two parts. The first part calculates all the parameters that are fixed by the geometry and do not depend on the flow or temperature. Then, a two-part iterative calculation is used to solve for the flows and temperatures. The inner iteration solves for coolant temperature given flow. The conservation of energy equations can be solved analytically for the five unknown temperatures given the three coolant flows; however, iteration is needed because the heat transfer coefficients depend on coolant temperature. The inner iteration consists of three steps: (1) assume the five temperatures, (2) solve for heat transfer coefficients given estimated flow and temperature, and (3) calculate new temperatures using conservation of energy and heat transfer through the heat exchanger tubes. This is repeated until the estimated and final temperatures are within an error criterion.

The outer iteration solves for flow. The method consists of the following steps: (1) assume flows in each of the three loops, (2) perform the inner iteration to calculate the temperatures given the flows, and (3) calculate the pressure balance around each loop from the flows and temperatures. If the pressure balance is not within an error tolerance about zero (meaning that the density driving head is not equal to

the friction losses in each loop), then flows are estimated again and the outer calculation loop is repeated. The outer flow estimation applies a relaxation factor to the change in the estimated flow to improve the stability of the convergence.

Natural circulation calculations sometimes encounter numerical difficulty due to the cancelation error associated with taking the difference between two nearly equal numbers, usually the difference between two temperatures or two densities. The natural circulation calculation anticipates the numerical problem and reformulates the balance equation in terms of temperature differences and density differences so that the subtraction is avoided in the spreadsheet calculation. Special property routines for density difference are programmed that compute the change in density given a starting temperature and a temperature change.

The spreadsheet is used to perform parametric studies to size a particular geometrical parameter in the design. For example, the maximum temperature of the primary salt is a key parameter in vessel creep estimates. Thus, a calculation might plot the core outlet temperature as a function of the elevation difference between the core and air heat exchangers in the DRACS loop.

The results of the DRACS sizing studies are input into the dynamic system model, where the transition from normal force-flow condition to the fully developed natural circulation flow condition is simulated. The time evolution of this transition plays an important role in determining the temperature response of the salt and the vessel. Additional inputs into the calculation include the expected response time to trigger a reactor shutdown, the response time of the control drives, and the decay heat produced within the reactor core.

2.2.2 Reactor Vessel Auxiliary Cooling System

The Reactor Vessel Auxiliary Cooling System (RVACS) works with the DRACS to remove heat from the vessel. During normal operation, the reactor vessel is maintained at approximately 650ºC by the inlet flow of the primary coolant. As the reactor makes the transition from normal forced flow to natural circulation flow, the reactor core, coolant, and vessel increase in temperature. Heat is continuously lost from the reactor vessel, and the heat loss rate is simply increased during loss of forced primary coolant flow.

The reactor vessel is positioned in the reactor silo, which is a large opening in the concrete reactor building. Steel structural members pass up through the reinforced concrete and support the reactor below the upper support flange. The vessel body extends into the reactor silo unsupported. Concrete surrounds the body of the reactor (everything but the upper flange and top hatch). The concrete within the reactor silo is lined with a stainless steel liner. An insulated enclosure structure is between the outer surface of the reactor vessel and the silo liner. This enclosure contains electrical heaters that are used to elevate the temperature of the vessel prior to salt loading. The insulation reduces the amount of electrical power required to heat the vessel and reduces parasitic loss during normal operation.

The silo liner is intimately connected to the silo concrete by stainless steel studs embedded in the concrete. The region between the liner and the insulated enclosure is filled with argon, as is the region between the insulated enclosure and the vessel.

The estimated major mass structures within the reactor silo are listed in Table 2 along with the estimated energy (in MJ) required to change the temperature of the structure by one degree Celsius. These masses are estimates, and the design of the insulated enclosure is less mature than that of the other components. The heat capacity of the fuel was calculated by D. Ilas[6] and includes the primary salt within the core coolant channels.

What the heated enclosure must heat depends on how the system is assembled. It is currently assumed that a dummy reactor core is loaded within the vessel prior to the salt being loaded. If the fuel, reflector, and internal structure are in the vessel, they must be heated and the time to temperature is increased. The

salt is by far the largest thermal capacitance, and once it is loaded the system responds slowly to heat input.

Table 3 lists the time to increase the temperature of (1) the reactor vessel only, (2) all system masses within the enclosure excluding the salt, and (3) those masses plus the salt mass within the vessel, assuming no parasitic heat loss. A 5-MW heat input will increase the vessel temperature 500ºC in approximately 7 hours. With the vessel dry and fully loaded (fuel, reflector, core. and structure), 5 MW of heat input would increase the temperature 500ºC in approximately 35 hours. To increase the system another 150ºC (to near the 650ºC operating temperature) after the salt is loaded will take an additional 25 hours with 5 MW of auxiliary heat, assuming no parasitic heat loss. Accounting for parasitic loss from the enclosure to the silo structure increases the times to temperature.

Table 2. Estimated masses and heat capacities of the major components within the reactor silo

	FliBe	SiC	Vessel	Reflector	Fuel	Argon	Enclosure	Liner
m3	375.3	39.7	56.3	146.0	263.4	180.5	8.9	4.7
Density	1960.0	2693.6	8860.0	1739.9		1.7	8000.0	8000.0
Mass (kg)	735,669.3	106,890.0	499,249.8	254,003.0		297.9	71056.9	37974.8
J/kg-K	2400.0	900.0	500.0	750.0		525.0	2400.0	2400.0
MJ/K	1765.6	96.2	249.6	190.5	556.7	0.2	170.5	91.1

Table 3. Estimate response times to heat input for the AHTR systems within the reactor silo

	Vessel	Within enclosure	Total system
MJ/K	249.6	1263.5	3029.3
MJ/S	5.0	5.0	5.0
Temperature rise	500.0	500.0	150.0
Hours	6.9	35.1	25.2

2.3 PRIMARY SYSTEM WARM-UP PRIOR TO OPERATION

The difference between warming the system with and without the DRACS being operational is shown in Fig. 13. These calculations estimate the temperature of the vessel and the two shield walls during a simulated system warm-up in which no heat is transferred to the intermediate heat transport system. At time T = 0 and following, 4 MW of heat is added to the heated, inner enclosure wall and the increasing temperature begins to heat both the reactor vessel and the shield wall. When the DRACS is not operational (the top plot), an equilibrium is reached in which the temperature of the vessel equals that of the enclosure and all of the heat is lost to the surrounding structure, which in this case, is assumed to be actively cooled to 27ºC. The system remains in this equilibrium until the reactor power is increased to 4 MW, at which time the temperature of the vessel increases above that of the heated shield.

When the reactor is started in this simulation, the auxiliary heat to the enclosure is terminated and a final equilibrium is reached in which the vessel loses heat to the inner wall of the enclosure, which in turn loses heat to the outer enclosure wall. The gaps between these structures and the gap between the outer

enclosure wall and the reactor silo liner are assumed to be filled with argon, but the radiation heat transfer between the surfaces is important. Natural circulation within the gaps has not yet been modeled, but it will increase heat transfer unless baffles are used to disrupt flow.

The size of the gaps can vary but, generally, the inner enclosure wall should be close to the reactor vessel and the distance to the outer enclosure wall increased. Clearance must be maintained for inspection and maintenance. The emissivity between the vessel and the inner wall should be high, and the emissivity between the other surfaces low.

A similar system warmup with the DRACS operational is shown in the lower graph in Fig. 13. In this case, the reactor vessel temperature remains below the inner enclosure wall temperature, and the heat loss from the heated wall is split into two directions. The DRACS system pulls heat from the vessel wall resulting in a lower overall vessel temperature when the auxiliary heat input is removed from the inner enclosure wall. In this case the temperature remains above the freezing temperature of the primary coolant salt, but with less margin.

Warmup with a 4 MW heated enclosure will take on the order of 10 days, depending on the insulating value of the wall. This is acceptable and probably desirable during the initial startup.

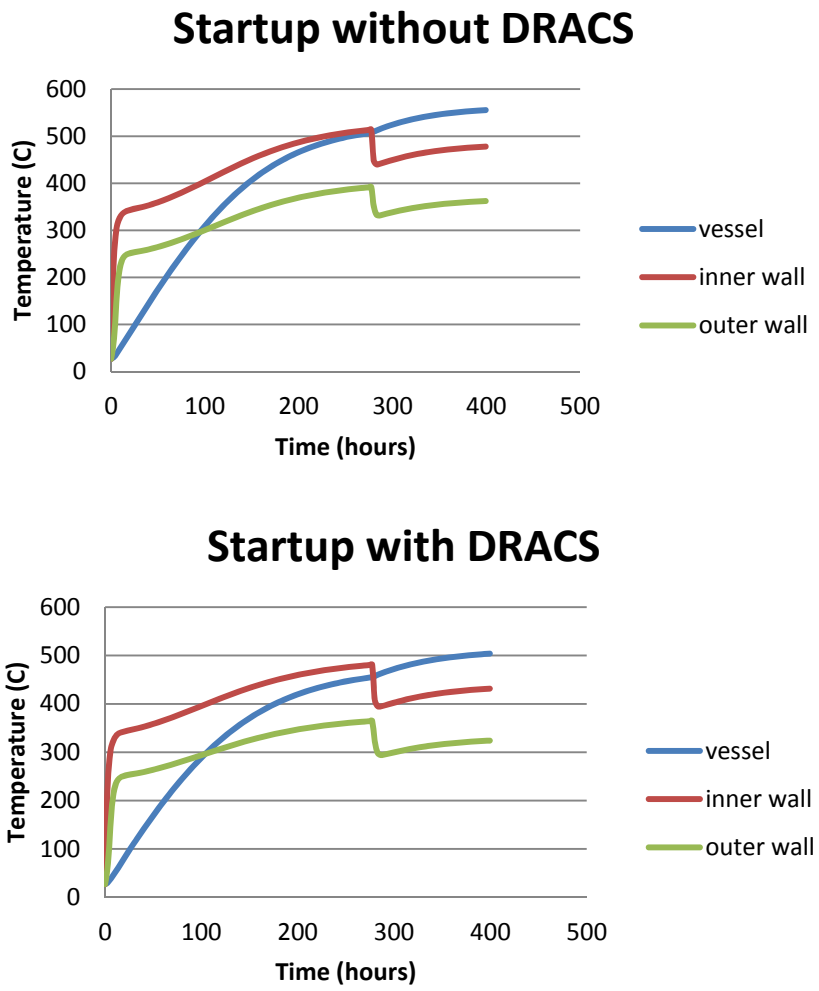

Fig. 13. Preliminary AHTR vessel and enclosure system response during warm-up.

The conceptual design of the heated enclosure is preliminary, but it plays an important role in system warmup, startup, and operation. During severe accidents with a loss-of-force-flow through the primary system, decay heat from the fuel will be dissipated by the DRACS and the RVACS. It is assumed that the RVACS will be housed between the heated enclosure and the reactor silo liner. The RVACS system is conceptually a flowing argon system. The argon is cooled by a refrigeration system located outside the reactor silo. The RVACS is not considered a safety system, and no credit is taken for it in withstanding accidents. The DRACS is designed as the safety-related heat removal system.

3. MODELING LANGUAGE AND DEVELOPMENT ENVIRONMENT

3.1 IMPLEMENTATION LANGUAGE: MODELICA

Modelica was chosen as the simulation language for the end-to-end system model. Modelica is a language developed specifically for modeling of physical systems. It is a modern language built on a causal modeling with mathematical equations and object-oriented constructs to facilitate reuse of modeling knowledge. The Modelica language is a product of an international cooperative effort to define an object-oriented language for modeling of generic physical models described by algebraic and differential equations. The *model*, which represents the behavior of a physical component, is described by a set of equations governing the dynamics.

The model of AHTR being developed in Modelica is more complicated than the Matlab model. The Modelica model includes three separate primary flow loops and three DRACS loops, and it explicitly models the flow through the primary vessel and the natural circulation-driven flows in each of the three independent DRACS systems.

3.2 DEVELOPMENT ENVIRONMENT: DYMOLA®

The Modelica language has built-in features and open-source-toolsets for modeling power systems. Systems are modeled by connecting “classes” of components in series or parallel and by specifying the important parameters of the components. Some examples of component classes are shown in Fig. 14. Fluids within the components are specified as well. A fluid is specified by defining the appropriate thermophysical properties, and solver routines use these properties to evaluate heat transfer coefficients, friction factors, and phase changes. The properties of water are already built into the system. Water has a complex set of properties that are modeled into the supercritical regime. The properties of the primary and intermediate salts used in AHTR had to be programmed into Modelica. Because the solver routines check essentially all of the thermophysical properties during execution, each property had to be developed and included for the salts added. So, while the solution might be expected to be more straightforward with salts that operate within well-behaved property regimes, the implementation of each salt is fairly complicated.

3.2.1 AHTR Media Libraries

The AHTR Media package defines the properties of materials used in the model implementations. Fluid media properties are constructed in multiple layers of abstraction: (1) the base layer and (2) the independent layer. The base layer, such as FLiBe_base and KFZrF4_base, are the abstracts classes—called Partial classes in Modelica, and implement the bases of property correlations. These base classes, in turn, inherit their semantic rules from PartialTwoPhaseMedium class. Figure 15 shows a partial list of fluid included in the AHTR Media library.

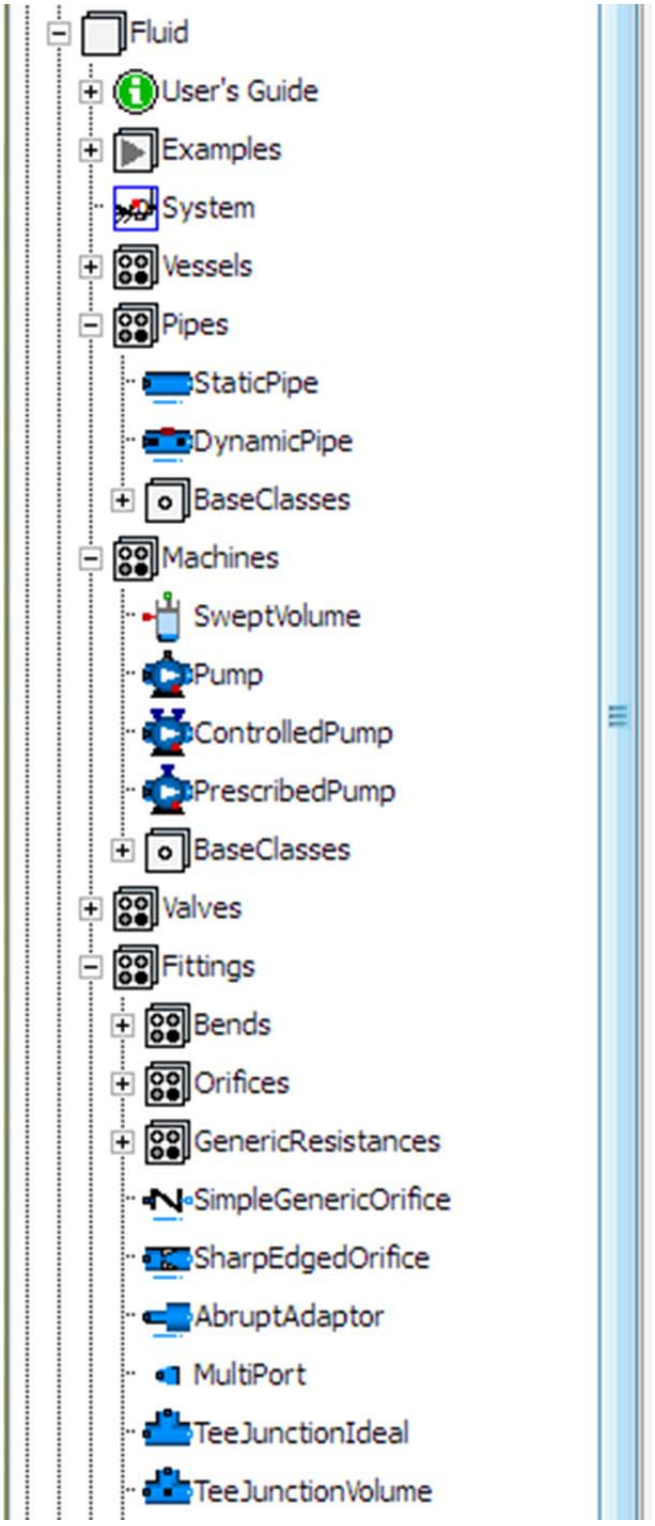

Fig. 14. Modelica fluid library comes standard in Modelica 3.2 language specification.

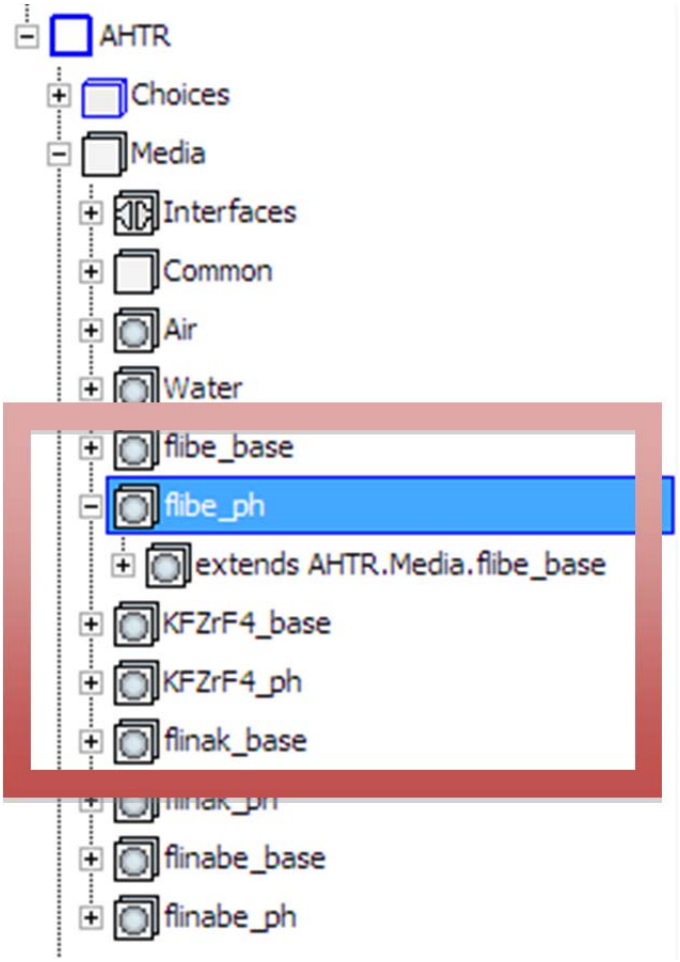

Fig. 15. FLiBe and KF-ZrF_4 salt property implementations within the AHTR Media package.

FLiBe_ph and KFZrF4_ph classes specify the independent variable to be used in the calculation of fluid properties. Pressure p and enthalpy h were chosen as the independent variables in this work for the implementation of fluid properties because selection of these variables exhibit higher stability for numerical calculations. An example of the callout for FLiBe is shown in Fig. 16.

```
package flibe_ph "Flibe properties explicit in p and h"
  extends AHTR.Media.flibe_base(
      ThermoStates=Choices.IndependentVariables.ph,
      final ph_explicit=true,
      final dT_explicit=false,
      final pT_explicit=false,
      smoothModel=false,
      onePhase=false);
  a;
end flibe_ph;
```

Fig. 16. FLiBe_ph class that specify independent variables for fluid properties (p and h).

Selected properties for FLiBe were implemented in the Modelica Media library within the AHTR package as shown in Table 4. Similar data is shown for KF-ZrF_4 in Table 5.

Table 4. Selected thermophysical properties for FLiBe

Physical property	Correlation	Unit	Source
Density	$\rho = \rho_T\,[1 + \kappa(P - P_o)]$ * $P_o = 6.367 \times 10^{-4}$ Pa	ρ (kg/m^3) P (Pa)	Cantor et al. (1968) Cantor (1973)
	$\rho_T = 2412.3 - 0.4884\,T$	ρ_T (kg/m^3) T (K)	Cantor et al. (1968)
Saturation line	$P_{sat} = 133.32 \times 10^{\left(9.04 - \frac{10500}{T}\right)}$	T (K)	Cantor et al. (1968)
Isothermal compressibility	$\kappa = 2.3 \times 10^{-11}\, e^{0.001\,T}$	κ (1/Pa) T (K)	* Derived from fundamental properties $\kappa = \frac{1}{\rho}\left(\frac{d\rho}{dP}\right)_T$
Coefficient of thermal expansion	$\beta = \frac{0.4884}{\rho_T} - \frac{0.001\,\kappa(P - P_o)}{1 + \kappa(P - P_o)}$	β (1/K) P (Pa)	* Derived from fundamental properties $\beta = \frac{1}{\rho}\left(\frac{d\rho}{dT}\right)_P$
Specific heat capacity	$c_p = 2386$	c_p (J/kgK)	Cantor et al. (1968)
Thermal conductivity	$k = 1.1$	k (W/mK)	Williams et al. (2004)
Dynamic viscosity	$\mu = 1.16 \times 10^{-4}\, e^{\frac{3755}{T}}$	T (K)	Cantor et al. (1968) Cantor (1973) Powers et al. (1963)

Table 5. Selected thermophysical properties for KF-ZrF_4

Physical property	Correlation	Unit	Source
Density	$\rho = \rho_T\,[1 + \kappa\,(P - P_o)]$	ρ (kg/m^3) P (Pa)	* P_o not available. Constants were set to the values of FLiBe
	$\rho_T = 3658.3 - 0.887\,T$	ρ_T (kg/m^3) T (K)	Williams et al. (2006)
Saturation line	$P_{sat} = 133.32 \times 10^{\left(9.04 - \frac{10500}{T}\right)}$	T (K)	* Data not available. Constants were set to the values of FLiBe
Isothermal compressibility	$\kappa = 2.3 \times 10^{-11}\, e^{0.001\,T}$	κ (1/Pa) T (K)	* Data not available. Constants were set to the values of FLiBe
Coefficient of thermal expansion	$\beta = \frac{0.887}{\rho_T} - \frac{0.001\,\kappa(P - P_o)}{1 + \kappa(P - P_o)}$	β (1/K) P (Pa)	* Derived from fundamental properties $\beta = \frac{1}{\rho}\left(\frac{d\rho}{dT}\right)_P$
Specific heat capacity	$c_p = 1050.18$	c_p (J/kgK)	Zucrow et al. (1976)
Thermal conductivity	$k = 0.45$	k (W/mK)	* Predicted at 700ºC
Dynamic viscosity	$\mu = 1.59 \times 10^{-4}\, e^{3179/T}$	μ (Pa s) T (K)	Williams et al. (2006)

Alloy N

Alloy 800H with an Alloy N vessel liner are the current AHTR primary vessel materials. Alloy N was originally developed at ORNL under the Molten Salt Reactor Program and used for the vessel and primary piping of the Molten Salt Reactor Experiment (MSRE). It is known to exhibit superior corrosion resistance characteristics to fluoride salts; however, Alloy N is not an approved material for high-temperature nuclear reactor components. Alloy 800H has an approved code case for 60-year operation as a high-temperature nuclear reactor material; however, it contains too much chromium for good fluoride salt compatibility. Alloy 800H with an Alloy N liner is assumed as the structural material combination for all primary and intermediate systems that come in contact with high-temperature salts unless Alloy N only is specified.

4. AHTR SYSTEMS MODELS

Within the Modelica environment, the AHTR plant has five top-level systems that dynamically interact with each other, as shown in Fig. 17. These systems include the following.

1. Reactor Core and the Primary Heat Transport System (PHTS)
2. Direct Reactor Auxiliary Coolant System (DRACS)
3. Secondary Heat Transport System (SHTS)
4. Power Conversion System (PCS), generator and electric grid
5. Ultimate Heat Sink (UHS)

Current emphasis is on the development of the primary system, including the passive heat removal systems, because these systems evolve from forced-flow during normal operation to natural circulation flow (including flow reversal) during accident situations. The primary system includes the parameters of interest from a safety perspective and is therefore modeled with the most detail. For AHTR, the primary vessel also stands out as a key safety indicator for the primary system. This is primarily due to the fact that the fuel in the AHTR has such a large temperature margin; the primary vessel becomes the limiting component that determines the available and useful life of the reactor. This fact requires that the primary vessel be modeled with ample fidelity to determine potential vulnerabilities of the component during key transients of interest, including complete loss of offsite power (LOOP) transients, which eventually leads to loss of forced flow (LOFF) in the primary and the secondary heat transport systems; turbine trip and generator trip transients; and anticipated transient without scram (ATWS).

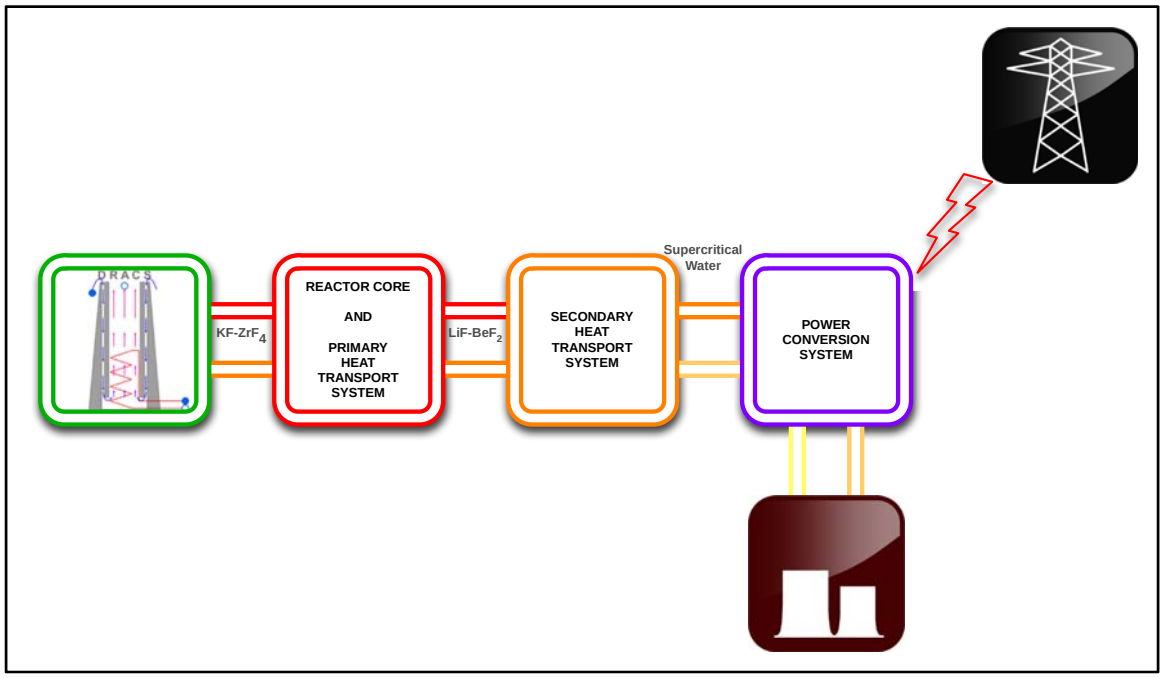

Fig. 17. Major system breakdown and connections for the AHTR.

4.1 AHTR PRIMARY SYSTEM FLOW LOOPS

This model currently represents six flow loops—three DRACS channels and three downcomer channels—in the AHTR primary vessel, as shown in Fig. 18. Each downcomer channel is connected to its dedicated salt pump. All six channels merge at the lower plenum before entering the reactor core. The rxLowerPlenum component model implements the mixing by performing mass and energy balances, that is, flow and enthalpy.

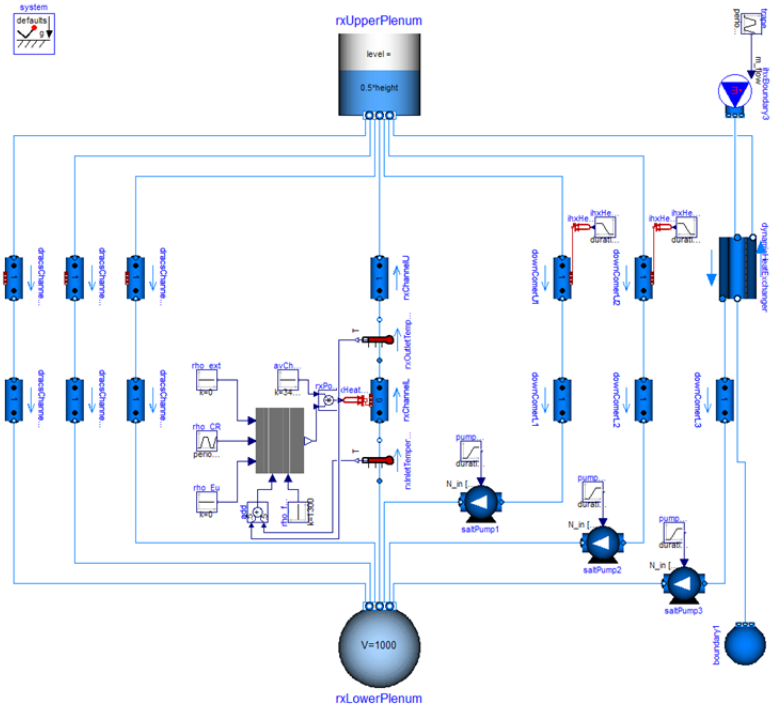

Fig. 18. Modelica representation of the Primary Heat Transport System for the AHTR.

The flow network includes an upper plenum, which also serves as an expansion tank for the primary fluid inventory. The rxUpperPlenum class, similarly, implements the mixing phenomenon by performing mass and energy balances. The rxUpperPlenum class also implements a slightly pressurized argon cover gas above the fluid-free surface.

The upper portion of the downcomer loops is connected to P-IHXs, which are currently implemented only as fixed heat rejection rate of one-third of the reactor power (i.e., approximately 1133 MW). In this particular implementation, DRACS heat rejection ports were disconnected to demonstrate heat rejection through the IHXs upon a LOFF event in the primary heat transport system.

4.2 REACTOR CORE

The reactor core is modeled as 24 separate nodes with fixed radial and axial power profiles imposed on them. Three inner zones are fueled regions, and most of the 3400 MW(t) is assumed to be generated within the 18 nodes comprising those zones. The outer zone represents an unfueled blanket region, and a selectable percentage of the reactor power is assumed to be generated within it due to secondary reactions. Each zone is made up of a fixed number of fuel bundles and associated coolant channels.

Each radial zone is modeled as a series of six axial nodes. The outlet temperature of a single channel in each radial zone is calculated, and the mixed temperature of the coolant in the upper plenum is calculated based on the number of channels modeled in each zone. The mass flow rate to each zone is adjustable within the model.

The reactor's negative temperature feedback is modeled using point kinetics with the temperature of a single central fuel channel used as temperature feedback. The negative temperature coefficient of reactivity, coupled with the fact that the mass of the fuel, vessel, and coolant is substantial, leads to inherently long response times for all credible transients that do not include a sudden loss of coolant. Because of long response times and large fuel temperature safety margins, reactor transient scenarios that occur quickly are difficult to postulate. It is more likely that transient scenarios in which the temperature slowly increases over periods of several days would be of primary concern. The Modelica graphical representation of the core inputs and output is shown in Fig. 19.

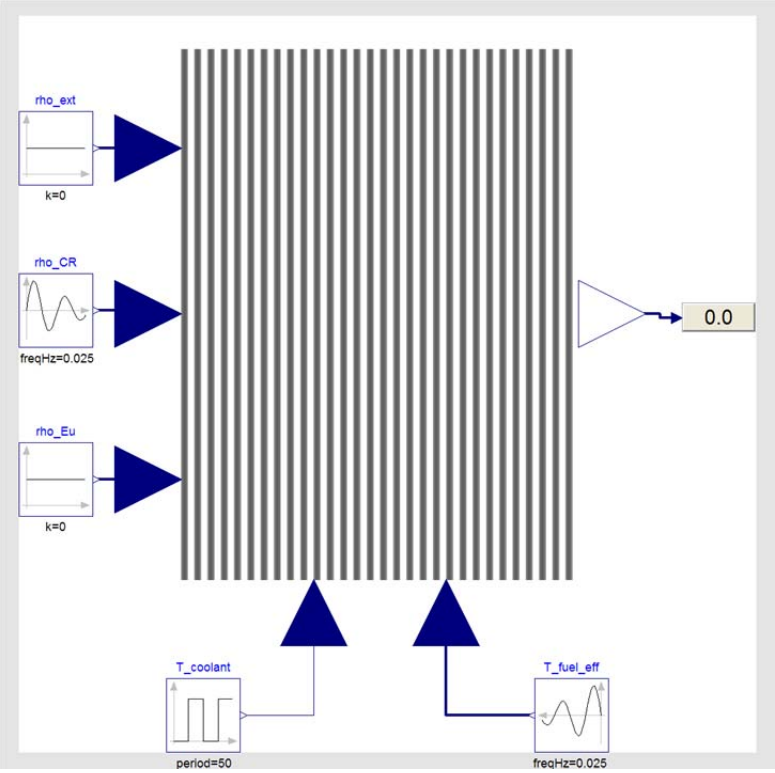

Fig. 19. Modelica graphical representation for the AHTR core model.

Reactor dynamics is modeled by six-precursor group point kinetics equations:

$$\frac{d}{dt}n(t) = \left(\frac{\rho(t)-\beta}{\Lambda}\right)n(t) + \sum_{i=1}^{6}\lambda_i\, c_i \tag{1.a}$$

$$\frac{d}{dt}\, c_i(t) = \left(\frac{\beta_i}{\Lambda}\right)n(t) - \lambda_i\, c_i(t) \qquad i = 1, \ldots, 6 \tag{1.b}$$

where n is the normalized neutron power, c is the neutron precursor concentration leading to a delayed neutron source, $\rho(t)$ is the total reactivity of the core, β is the fraction of delayed neutrons, λ is the decay constant, and Λ is the mean neutron generation time.

The reactivity feedback is modeled taking into account a number of feedback mechanisms. These include (1) fuel Doppler feedback (ρ_f) and (2) coolant density feedback (ρ_c). Two sources of reactivity control inputs are provided: (1) control blade reactivity (ρ_{CR}) and (2) europium (ρ_{Eu}) negative reactivity as neutron poison. The feedback equations are as follows:

$$\rho(t) = \rho_{CR} + \rho_f(t) + \rho_c(t) + \rho_{Eu}(t) \quad (2.a)$$

$$\begin{cases} \rho_f(t) = \alpha_f\left(T_e - T_{e_o}\right) & (2.b) \\ \rho_c(t) = \alpha_c\left(\dfrac{1}{\nu_c} - \dfrac{1}{\nu_{c_o}}\right) & (2.c) \\ \rho_{Eu}(t) = \alpha_{Eu}\left(C_{Eu} - C_{Eu_o}\right) & (2.d) \end{cases}$$

where T_e and T_{e_o} are the instantaneous and reference effective fuel temperatures, respectively, obtained from the fuel thermal conduction model explained in the next section; ν_c and ν_{c0} are the instantaneous and reference specific volumes of the primary coolant; C_{Eu} and C_{Eu_o} are the instantaneous and reference europium concentration in the coolant. Europium can be used as a means to control excess initial reactivity in the core. This variable is created to provide long-term burnup reactivity control; however, it is not being used at this point, and is simply assigned zero.

A dialog box is provided, as shown in Fig. 20, to allow users to enter design-specific control parameters for the reactor dynamics class. Each parameter is assigned a default value (or values) shown as greyed-out entries, as indicated in Fig. 20.

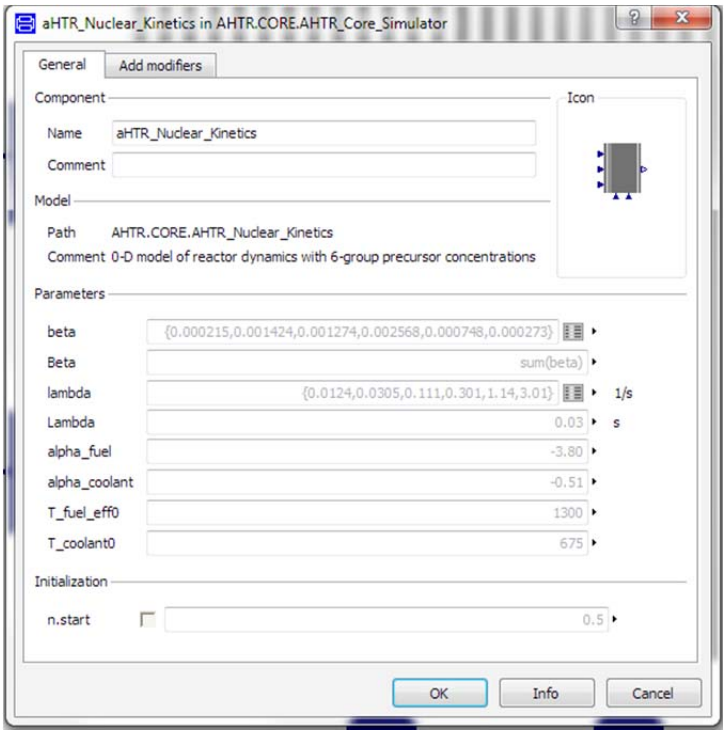

Fig. 20. Dialog box to input design-specific parameters for reactor kinetics calculations.

4.2.1 Fuel Thermal Model

Within the plate fuel element, the TRISO fuel particles are distributed in two stripes by central carbonaceous material. This design has neutronic advantages, allowing better moderation as well as thermal-hydraulic considerations that allow better cooling. An ~0.1-mm-thick sleeve of carbonaceous material separates each fuel stripe from the FLiBe coolant, preventing individual fuel particles from eroding away. The cross-sectional drawing of the fuel plank is shown in Fig. 21.

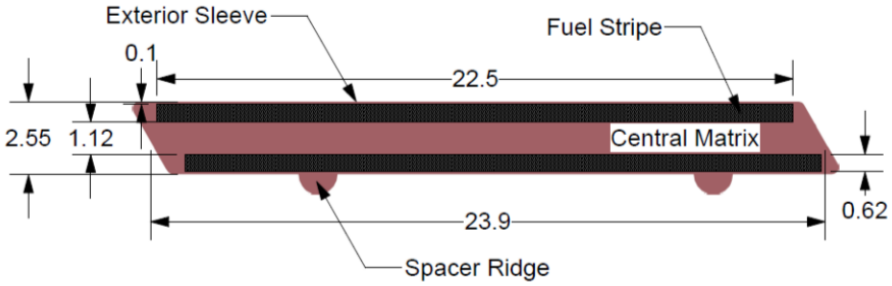

Fig. 21. Geometry of a fuel plank for thermal model (quantities in mm).

Fuel thermal model class implements the dynamics of the conduction equation in Cartesian geometry. The thermal model of the fuel plank is shown in Fig. 22, which represents half of the plank, assuming thermal symmetry.

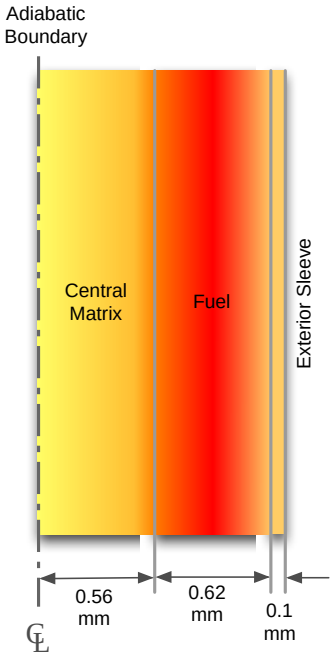

Fig. 22. Dimensions for the fuel thermal conduction model.

The fuel is modeled in three regions: (1) central matrix, (2) fuel stripe, and (3) exterior sleeve. The time-dependent conduction equations for each region are as follows:

$$k_{CM}\frac{\partial^2 T_{CM}}{\partial x^2}=0 \qquad \text{Central matrix} \qquad (3.a)$$

$$\rho_f c_{p_f}\frac{\partial T_f}{\partial t}=k_f\frac{\partial^2 T_f}{\partial x^2}+q''' \qquad \text{Fuel} \qquad (3.b)$$

$$k_s\frac{\partial^2 T_s}{\partial x^2}=0 \qquad \text{Exterior sleeve} \qquad (3.c)$$

where k is thermal conductivity, T is temperature, ρ is material density, c_p is specific heat capacity, and q''' is the heat generation rate density in the fuel, which is considered uniform. Subscripts CM, f, and s represent the central matrix, fuel, and the exterior sleeve, respectively. The solution of the conduction equation is provided in Appendix A.

These equations are solved subject to an adiabatic boundary condition in the centerline (i.e., zero heat flux), and sleeve-coolant interface convection heat flux, represented as

$$q'' = h\left(T_{s_o}-\overline{T}_c\right)$$

where q_s'' is the heat flux at sleeve-coolant interface, T_{s_o} is the sleeve surface temperature, and $\overline{T}_c$ is the mean coolant temperature. In addition to these boundary conditions, the system of equations is subject to an interfacial continuity condition for both the temperature and heat flux.

A common practice in thermal fuel models of light water reactor (LWR) fuels is to have multiple zones for the fuel region. This is extremely important for oxide fuels where significant density variations are observed due to sintering effect, which results in significant differences in fuel thermal conductivity, k_f. In this particular fuel design, fuel is dispersed virtually uniformly within the fuel region. Because individual fuel elements are contained within TRISO particles, zoning phenomenon is not expected. Therefore, the fuel region is represented by one zone only.

The effective fuel temperature for the slab geometry is calculated by

$$T_e = \frac{1}{2}T_{f_{\min}} + \frac{1}{2}T_{f_{\max}} \qquad (4)$$

where $T_{f_{\min}}$ and $T_{f_{\max}}$ are minimum and maximum fuel temperatures, respectively. The effective fuel temperature is used to calculate the Doppler reactivity feedback contribution on dynamics.

4.2.2 Heat Exchangers

The P-IHXs are assumed to be enhanced tube and shell heat exchangers. The sizing and modeling of these heat exchangers is straightforward in Dymola. The equipment used to transfer the heat from the intermediate salt to the water in the power conversion system is different from the salt-to-salt heat exchangers and from that used for coal-fired plants. The modeling of the Supercritical Water Generators (SCWGs) assumed for the AHTR is therefore a more difficult development activity.

In the SCWG, the water passes through parallel tube arrangements in a once-through arrangement and the heating fluid passes over the outer surface. For the AHTR, this places the intermediate system salt on the shell side of what is essentially a traditional tube-and-shell heat exchanger.

The water side of the SCWG is a once-through “boiler” arrangement, although in a supercritical system no boiling actually occurs. Water enters the tubes “compressed” (at pressures above the critical pressure but below critical temperature) from the condenser and feedwater heater arrangement. As the water increases in temperature and passes into the supercritical phase, the density, specific heat, and viscosity change significantly. The heat transfer coefficient on the inside of the tubes increases during this

transition phase and can peak at values ranging from 12,000 to 50,000 W/m^2-K, depending on flow and tube surface conditions. Beyond the transition area, the heat transfer coefficient gradually stabilizes and decreases. Values ranging from 5000 to 4000 W/m^2-K are typical.

Alloy N has been selected as the baseline design material for the interface between the intermediate salt and the supercritical water. The flow conditions on the shell side of the SCWG are currently set to be equal to those in the P-IHX. The wall thickness of the tubes, however, must be increased over those in the P-IHX because of the high pressure on the water side.

The full flow of supercritical water passes from the SCWG to the high-pressure turbine (HPT) and returns to the SCWG as traditional steam. The steam is reheated, typically to the same exit temperature as the supercritical water, in a separate set of tubes. The total heat transferred into these two loops is equal to that lost by the intermediate salt, and the balance is roughly three-quarters of the heat going to the supercritical tubes and one-quarter of the heat going to the reheat tubes.

In the dual power train system, half of the heat transferred to the intermediate loop salt is transferred to each SCWG—approximately 1700 MW(t). The flow rate of supercritical water within the power conversion loop required to generate power has been estimated to be approximately 0.74 kg/s of flow per megawatt of power generated at the turbine shaft. This scaling factor was taken from the operation of existing supercritical plants. The flow rate for each ~750 MW(e) power train of the AHTR is approximately 590 kg/s. The water enters the generator at 320°C and exits at 650°C.

The peak temperature of the intermediate coolant is 675°C, and it loses 75°C through the SCWG. Thus, the flow rate of the intermediate salt through the shell side of the supercritical water generator is 21,600 kg/s, and the average temperature of the salt is 637.5°C. The Log-Mean Temperature Difference (LMTD) for this arrangement is 105°C, which is higher than that available in the P-IHX.

The ShellAndTubeHeatExchanger class implements an abstract shell-and-tube heat exchanger model for use in integrated system models. The icon representing this in the model is shown in Fig. 23.

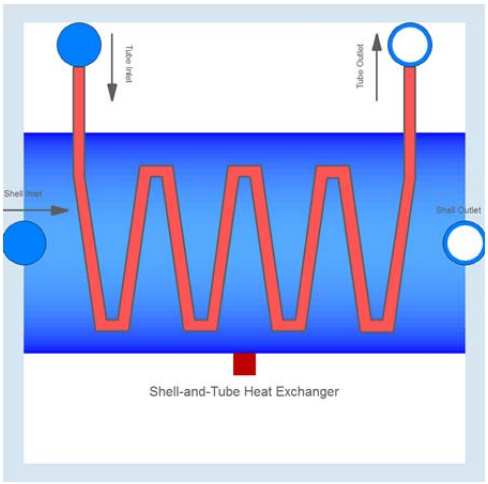

Fig. 23. Icon representing a reconfigurable ShellAndTubeHeatExchanger class.

The heat exchange is modeled through two independent flow channels—that is, the shell side and the tube side—that thermally interact through a metal wall, as illustrated in Fig. 24. The way the ports are connected determines whether the heat exchanger is in a counter-flow or parallel flow configuration. Each flow channel, implemented using the Pipe class, includes four interior flow nodes that internally perform mass, momentum and energy balances.

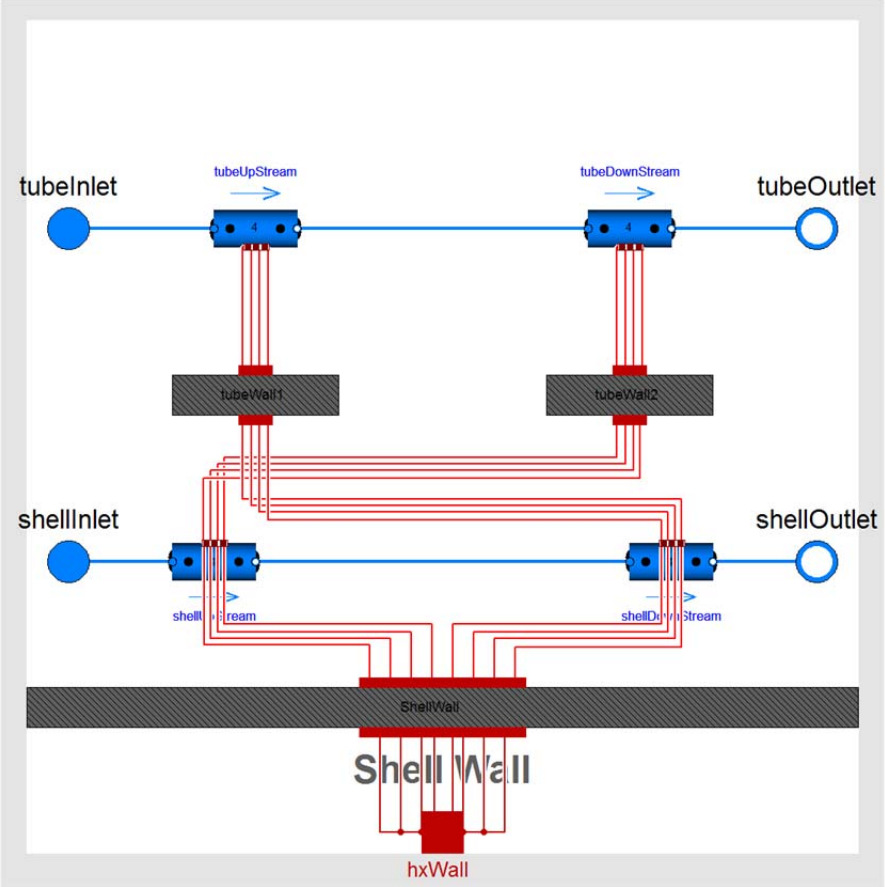

Fig. 24. Modelica model that shows the implementation of the ShellAndTubeHeatExchanger class based on the components provided in the Modelica Fluid package.

The shell side of the heat exchanger is also thermally connected to the ShellWall class that implements an eight-node thermal model of the heat exchanger outer shell. The hxWall port allows connection of a thermal element, which can be used as a boundary condition. If no connection is made, the class assumes an adiabatic boundary condition, which means ideal insulation of the heat exchanger. A fixed heat flux boundary condition with a negative value corresponds to constant parasitic heat loss through the insulation material, and heat loss to the environment can be modeled as a resistance to heat flow based on heat exchanger and ambient temperature differences.

The design-specific parameters of the ShellAndTubeHeatExchanger class can be input using the dialog box, as shown in Fig. 25.

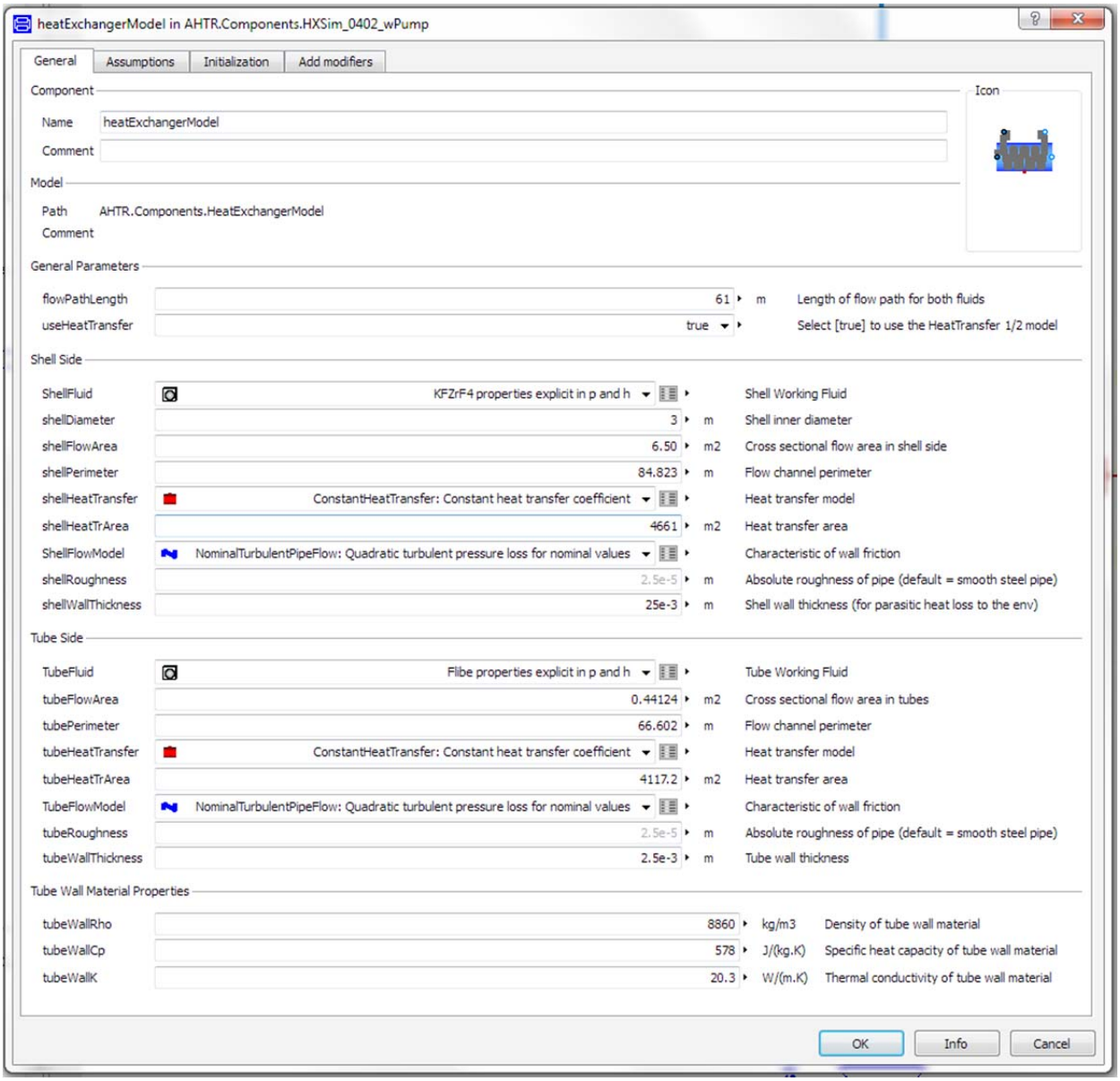

Fig. 25. Dialog box for the heat exchanger model to input major design specifications.

The component parameters can be initialized using *Initialization* tab in the same dialog box, as shown in Fig. 26.

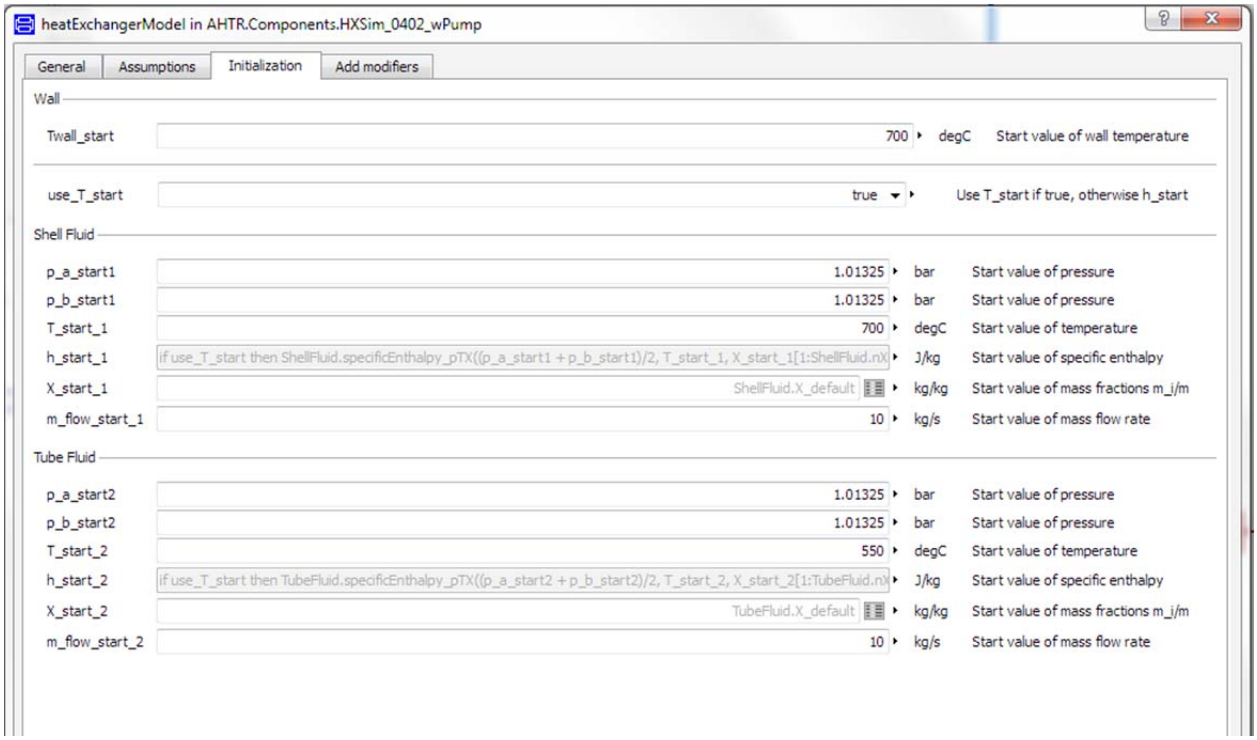

Fig. 26. Dialog box for the heat exchanger model to input initialization parameters for the component.

4.2.3 Pumps

The primary pumps are simple models. Electric motors power the pumps. The important pump parameter related to system transient response is the coastdown time of a pump after it loses power. The coastdown time is related to angular momentum, which is the principal pump design parameter that is varied in reactor response studies.

The pump model was directly inherited from the Modelica.Fluid package and is used to model the three primary and three intermediate salt pumps. The primary pumps are all assumed to be identical. The intermediate pumps are as well, and they are similar to the primary pumps. The primary difference is the nominal flow rate and the coastdown time.

4.3 INTERMEDIATE HEAT TRANSPORT SYSTEM

The primary system ends and the intermediate loops begin at the P-IHXs within the reactor containment building (RCB). The intermediate salt passes through the containment boundary and transports the heat from the primary system to the power conversion system. The nominal distance between these systems is currently set at 100 m. The intermediate piping within the RCB extends from the P-IHX to an interface between the reactor building and the tunnel. This interface provides seismic isolation between the intermediate and the primary systems. The two intermediate loops that extend from the side of the reactor have significant bends and are approximately 40 m in length within the reactor building. The third loop is shorter and more directly connected to the interface. Outside of the reactor building, the piping is mostly straight and it runs in an accessible covered tunnel between the buildings.

The intermediate system salt is KF-ZrF_4, which has a melting temperature near 400°C. The intermediate system, like the primary system, must be heated. A heated salt storage vessel is also required. Pressure diaphragms are required on the intermediate loop to prevent any power-conversion-triggered pressure transients from propagating to the primary coolant loop. Surges would direct intermediate salt flow to the salt storage tank.

The intermediate system makes a transition from three primary loops to two power conversion trains. This is accomplished by blending the high-temperature intermediate salt into a common header from which the two supercritical water generator and reheat (SCWG) units are fed.

The temperature change of the intermediate salt through the P-IHX was set at 75°C to reduce flow rate requirements. The heat capacity of KF-ZrF_4 is 1.05 J/g-K, and approximately 14,400 kg/s of KF-ZrF_4 flows through each of the three legs of the intermediate system for a total flow rate of 43,200 kg/s. This flow is split into two flow streams of 21,600 kg/s to feed the SCWGs.

The pipes between the P-IHX and the pumps and between the pumps and the vessel have an inner diameter of 1.24 m. These pipes will need to expand and contract with changing temperature. The heat exchangers and pumps will either need to move to accommodate stresses in the piping or the piping will have to bend to accommodate them. The size of the required bends would be large for a system operating between ambient temperature and 700°C; therefore, commercially available expandable bellows are used at each bend in the intermediate loop within the reactor building. This allows the elbows in the piping to be fixed and the straight piping runs to expand linearly along a fixed axis. Each joint is capable of expanding approximately 7.5 cm to 15 cm.

Electrical power to the pump motors is used to adjust flow in the three intermediate loops. Flow balancing valves, placed either beyond the hot-leg manifold or after the SCWGs, balance flow of intermediate salt between the two SCWGs. These valves have partial restriction for flow balancing and do not have a sealing requirement. Figure 27 shows a schematic of the major components comprising the power system.

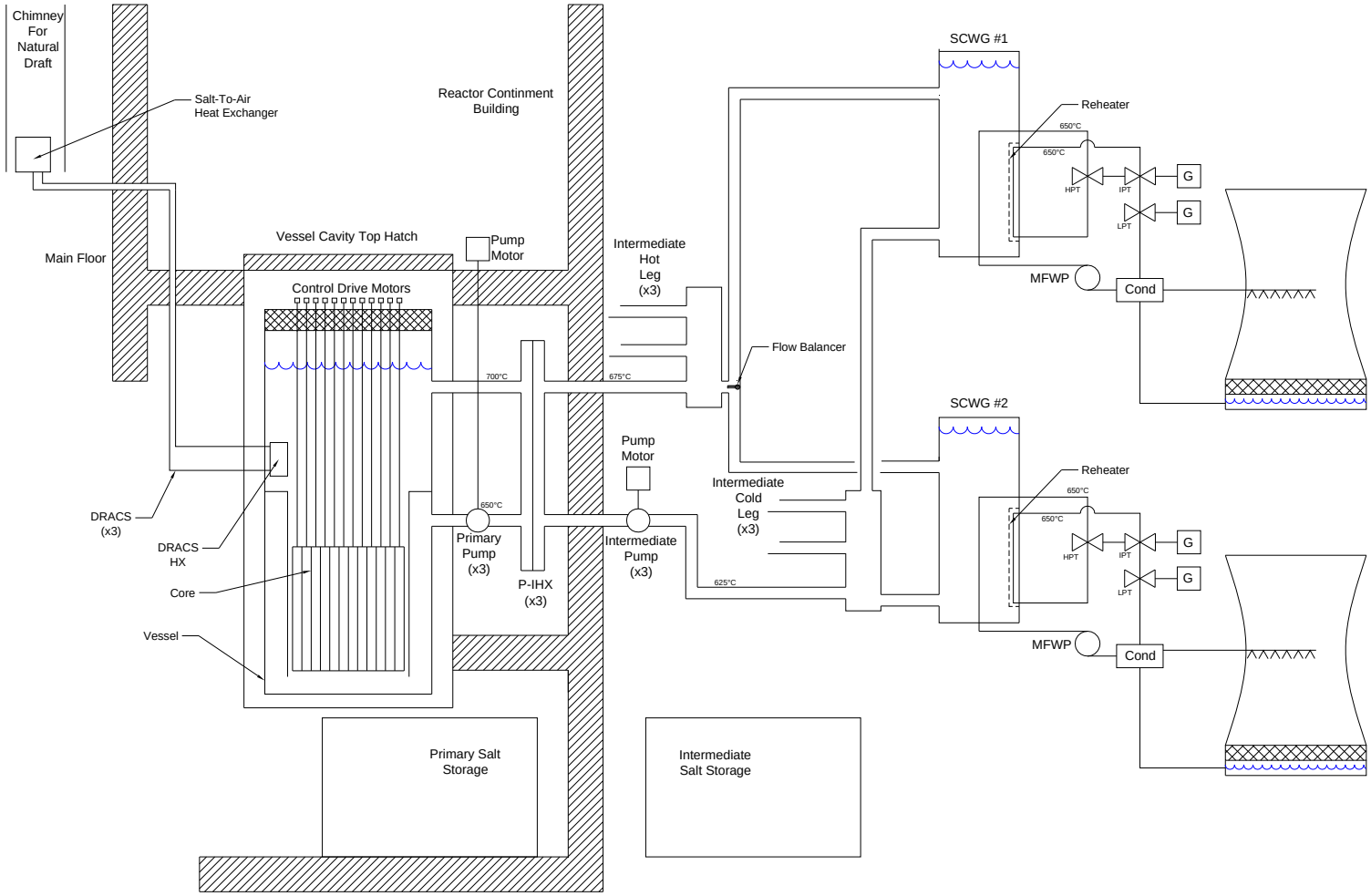

Fig. 27. Schematic of the flow loops of the ~1500 MW(e) AHTR with hybrid heat rejection.

5. NATURAL CIRCULATION AND FLOW REVERSAL

As component models are being developed, basic system models are created to test the fidelity of the models as well as the fidelity of the built-in numerical integration algorithms. The following sections show the results from of a subset of system models based on the standard component models as well as the models developed specifically for this project.

5.1 ONSET OF NATURAL CIRCULATION

A simple flow network model was developed to test and demonstrate the simulation of flow-reversal and natural-circulation phenomena in Dymola/Modelica, as shown in Fig. 28. This model includes four flow channels, using the `Pipe` class in the Modelica.Fluid package, a pump, and an expansion tank. The pump is tripped at $t = 600\ s$ with a coastdown period of 50 s. It assumes that the lower-right quadrant of the network is at a fixed temperature, while the upper-left quadrant rejects heat at a constant rate.

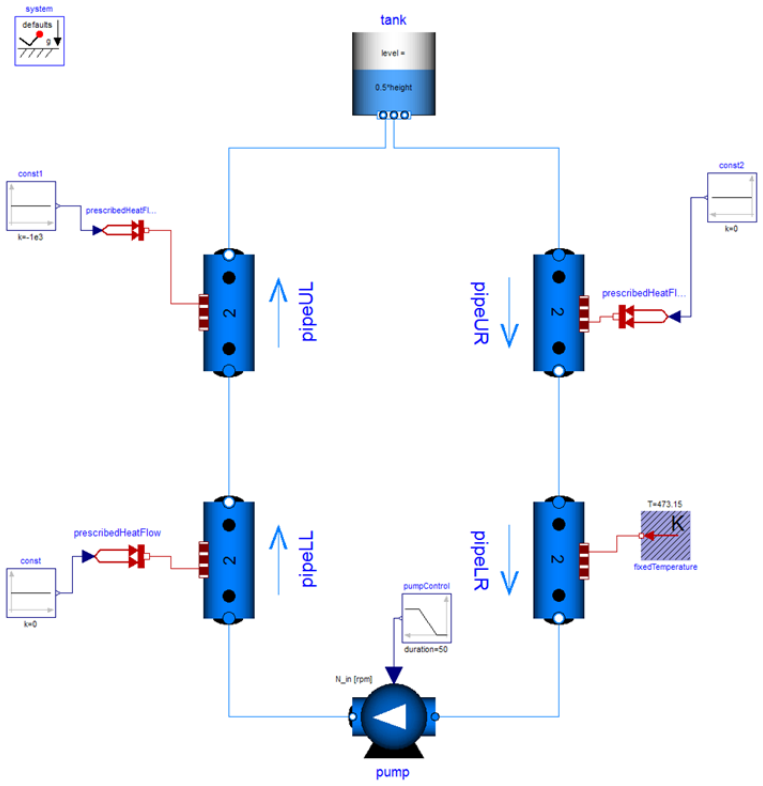

Fig. 28. Modelica model of a flow network to demonstrate the flow-reversal and natural circulation phenomena.

Upon the loss of forced flow, the flow rate reduces rapidly due to friction losses as well as growing dominance of buoyant forces in the opposite direction. Eventually, buoyant forces dominate and reverse the flow. The flow in the reverse direction exhibits overshoot because the density gradient is higher due to the coolant residing in the cooled section a longer time as the velocity slows, stops, and restarts in the

opposite direction. The flow approaches steady state within an hour as fluid temperatures reach steady-state values. The simulation results as shown in Fig. 29.

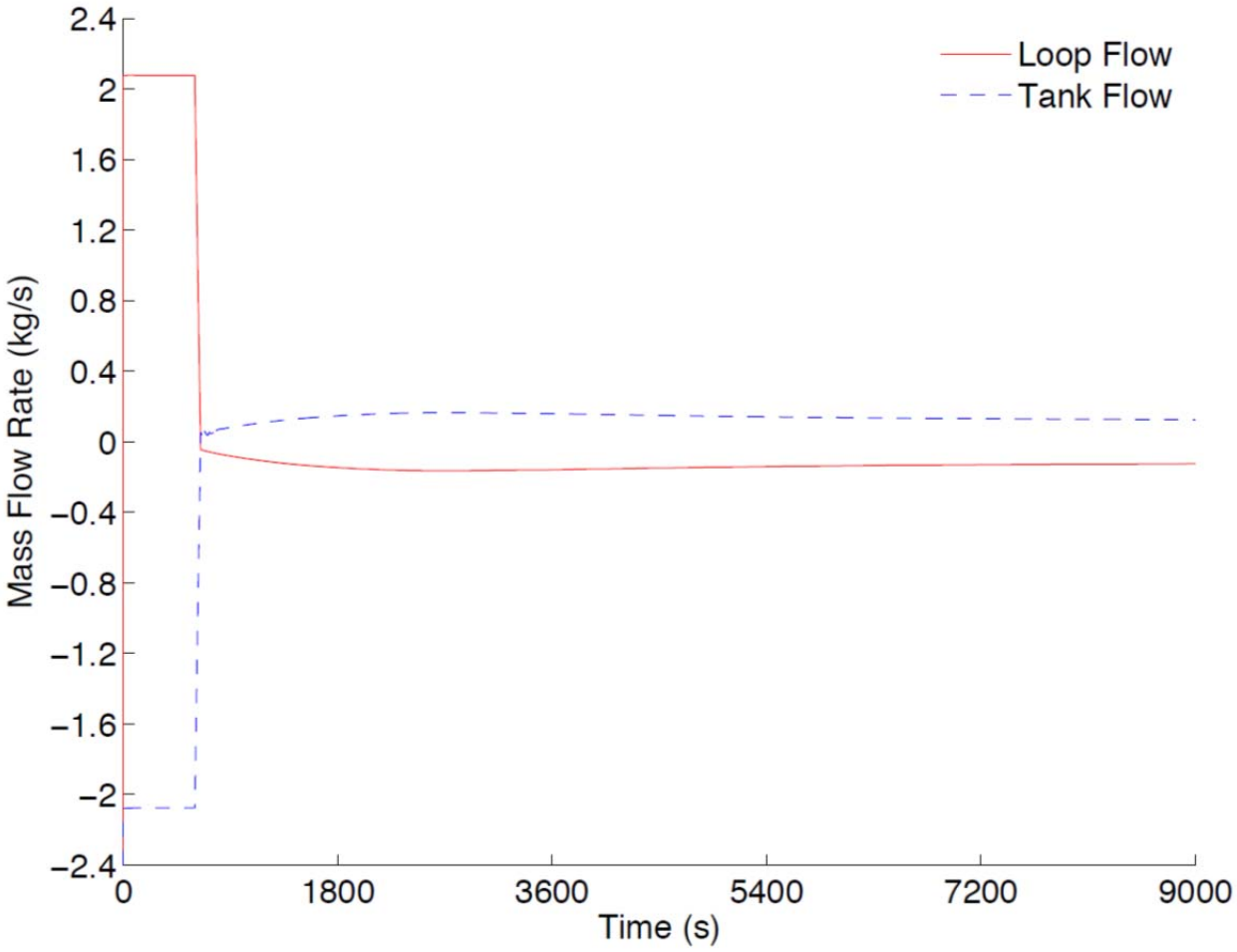

Fig. 29. Results of the simulation that shows a pump trip event and the subsequent onset of natural circulation including flow reversal.

6. CONCLUSIONS AND FUTURE ACTIVITIES

The design of the AHTR 3400 MW(t) power system is progressing, and the dynamic system models necessary to study plant operation, performance and safety are beginning to inform the design. Steady-state calculations are used to size equipment for nominal performance, and the design parameters from these calculations are fed into dynamic system models. MatLab Simulink-based models were developed in 2010–2011 and have been updated with current design parameters for the AHTR reactor primary system. This model has a simplified representation of the primary coolant flow through the reactor vessel and core and is used mainly to model the flow of heat to and from the reactor vessel during warm-up, startup, and transient operation. This model uses a fixed boundary condition on the secondary side of the P-IHX to represent heat loss from the primary system to the intermediate heat transfer loop. It can be configured such that no heat is lost to the intermediate loop, in which case the model estimates energy flows within the primary system, the reactor building, and to the environment through the DRACS system. This model is used to study the characteristics of the heated enclosure between the reactor vessel and the steel and concrete of the reactor silo. The model predicts that approximately 4 MW of thermal power within the heated enclosure can heat a fully loaded primary system (fuel and salt) to operating temperatures in approximately 10 days.

A more sophisticated dynamic system model is being developed in the Modelica modeling language. This model utilizes a representation of the complex flow geometry within the pressure vessel and includes flow models of the DRACS passive heat removal system. The Modelica-based model is capable of modeling transitions from nominal full-power operation to fully developed natural circulation-driven flow within the primary system, including the DRACS. Steady-state calculations are used to size the DRACS heat exchangers. The piping runs between the heat exchangers are directly influenced by the reactor building layout, and this information is used in both the steady-state analyses and the dynamic system model.

Results of the performance models will continue to inform the design process. The Simulink model will be used to validate the initial performance of the Modelica-based model and eventually its use will be phased out. Prior to the September project report the Dymola simulation will be extended to include representations of the power conversion system and the ultimate heat rejection system. The end-to-end performance model will be used to study system transient response to anticipated off-normal operating events as a function of specific design variables including, but not limited to, the following:

1. downcomer gap,
2. pump coast down time,
3. fluidic diode performance, and
4. reactor shutdown trip conditions.

An initial list of transient scenarios and design basis accidents for the AHTR system will be developed, and the probability of initiating events and the severity of the resulting consequences estimated. A more meaningful accident progression analysis will be completed as the design evolves and matures. In the absence of this information, some transient scenarios have been proposed for consideration, including reactivity insertion events, individual primary and intermediate pump failures, LOOP, and in the power conversion system, the loss of a turbine or generator.

7. REFERENCES

1. D. E. Holcomb, F. J. Peretz, and A. L. Qualls, *Advanced High Temperature Reactor Systems and Economic Analysis—September 2011 Status*, ORNL/TM-2011/364, Oak Ridge National Laboratory, Oak Ridge, TN, September 30, 2011.
2. D. E. Holcomb et al., *Core and Refueling Design Studies for the Advanced High Temperature Reactor*, ORNL/TM-2011/365, Oak Ridge National Laboratory, Oak Ridge, TN, September 2011.
3. D. E. Holcomb et al., "Current Status of the Advanced High Temperature Reactor," to be published in the *Proceedings of the 2012 International Congress on the Advances in Nuclear Power Plants (ICAPP '12)*, Chicago, IL, June 24–28, 2012.
4. R. E. Thoma and W. R. Grimes, *Phase Equilibrium Diagrams for Molten Salt Systems*, ORNL-2295, Oak Ridge National Laboratory (1957); and A. V. Novoselova, Yu. M. Korenev, and Yu. P. Simanov, *Dokl. Akad. Nauk SSSR* **139**(4), 892–894 (1961).
5. W. Ren, G. Muralidharan, D. F. Wilson, and D. E. Holcomb, "Considerations of Alloy N for Fluoride Salt-Cooled High-Temperature Reactor Applications," *Proceedings of the ASME 2011 Pressure Vessels & Piping Division Conference PVP2011*, July 17–21, 2011, Baltimore, MD.

APPENDIX A

DYMOLA

Dymola® is based on the use of Modelica models. The Dymola application has a built-in symbolic translator for Modelica model equations to generate C-codes for direct simulation as illustrated in Fig. A-1. The C-code can be executed either directly from the Dymola user interface or a standalone application. The code can also be accessed from MATLAB/Simulink to perform hardware-in-the-loop simulations.

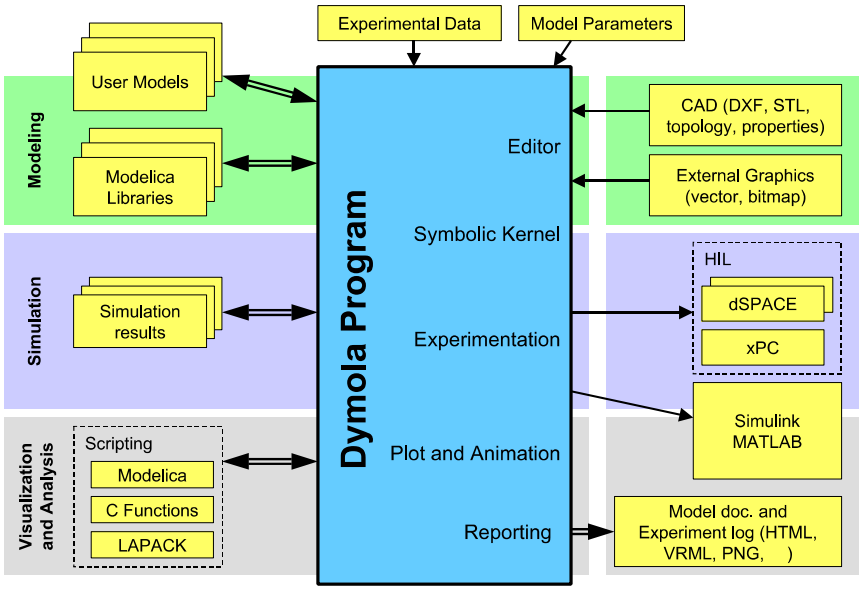

Fig. A-1. The architecture of the Dymola® application.

The Modelica Language Specification (Modelica 2005) defines how a Modelica model shall be mapped into a mathematical description as a mixed system of *differential-algebraic equations* (DAE) and discrete equations with Real, Integer, and Boolean variables as unknowns. No general-purpose solvers are provided for such problems. There are numerical DAE solvers, which could be used to solve the continuous part. However, if a DAE solver is used directly to solve the original model equations, the simulation will be slow and initialization might be not possible for high-index systems.

To solve this common problem, Dymola first performs a symbolic transformation of model equations into a form that is better suited for numerical solvers. Dymola converts the DAE system of equations symbolically to ordinary differential equations in state-space form; that is, it solves for the derivatives. Efficient graph-theoretical algorithms are used to determine which variables to solve for in each equation, and to find minimal systems of equations to be solved simultaneously (algebraic loops). The equations are then, if possible, solved symbolically, and an executable code is generated for efficient numeric solution. Discontinuous equations are properly handled by translation to state or time events as required by numerical integration routines.

EQUATION SORTING AND TREATMENT OF ALGEBRAIC LOOPS

The behavior of a Modelica model is defined in terms of genuine equations. The translator must assign an equation for each variable as part of the sorting procedure, which also identifies algebraic loops. To be able to process problems with thousands of unknowns, Dymola identifies which variables appear in each equation rather than how they appear. This information is represented in a structure called a *Jacobian*. The sorting procedure is to order unknowns and equations to make the *structure Jacobian* become Block Lower Triangular (BLT). A BLT partitioning reveals the structure of a problem. It decomposes a problem into sub-problems, which can be solved in sequence. There are efficient algorithms for constructing the BLT partitions with diagonal blocks of minimum size—with respect to permutation of equations and variables. Each non-scalar block on the diagonal constitutes an algebraic loop. This sorting procedure identifies all algebraic loops in their minimal form that is mathematically unique.

REDUCTION OF SIZE AND COMPLEXITY

From the BLT partition it is possible to find unknowns that actually are constant and can be calculated and substituted at translation. This procedure drastically reduces the complexity of the problem that has to be solved numerically. It means that cancellations are identified during the symbolic translation phase, and some terms in the overall system of equations may disappear. This in turn may decompose existing algebraic loops, which are numerically problematic for stable solutions, into smaller loops. Under certain conditions, some algebraic loops may be completely eliminated.

A linear small algebraic loop is solved symbolically. Otherwise, a code for efficient numeric solution is generated. In order to obtain efficient simulation, it is very important to reduce the size of the problem sent to a numerical solver. The work to solve a system of equations increases rapidly with the number of unknowns, because the number of operations is proportional to the cube of the number of unknowns.

When using Newton methods for nonlinear equation systems, it is necessary to calculate the *Jacobian* matrix. If this is made numerically from residuals, then n residual calculations are needed, where n is the number of variables in the simulation. Dymola, however, provides analytic Jacobians that are more accurate and much less computationally demanding. The Modelica language also provides facilities to provide derivatives for external functions.

INDEX REDUCTION

When solving an ordinary differential equation (ODE) the problem is to integrate, that is, to calculate the states when the derivatives are given. Solving a DAE may also include differentiation, that is, to calculate the derivatives of given variables. Such a DAE is said to have *high index*. It means that the number of states needed for a model is less than the number of variables appearing differentiated. The number of states is equal to the number of independent initial conditions that can be imposed. High-index DAEs are typically obtained because of constraints between models. To support reuse, model components are developed to be “general.” Their behavior is restricted when they are used to build a model and connected to other components.

The reliability of a direct numerical solution is related to the number of differentiations needed to transform the system algebraically into ODE form. Modern numerical integration algorithms for DAEs, such as used by most simulators, can handle systems where equations needed to be at most differentiated once. However, reliable direct numerical solutions for non-linear systems are not known if two or more differentiations are required. Furthermore, if mixed continuous and discrete systems are solved, the hybrid DAE must be initialized at every event instant. In this case, it is in general not sufficient to just fulfill the original DAE. Instead, some differentiated equations have to be fulfilled, in order that the initialization is

consistent. Direct numerical methods have problems at events to determine consistent restart conditions of higher index systems.

Dymola transforms higher index problems by differentiating equations *analytically*. This algorithm is based on the structure of the equations. For large problems, a structural analysis is the only feasible approach. Selection of which variables to use as state variables is done statically in the translation phase. In more complicated cases, state variable selection can be done during simulation.

SOLUTION OF CONDUCTION EQUATION

The homogenous time-dependent heat equation—also called conduction equation—is represented as follows:

$$u_t = c^2 u_{xx} \tag{A.1}$$

where $u_t = \frac{\partial u}{\partial t}$ and $u_{xx} = \frac{\partial^2 u}{\partial x^2}$, which is subject to the boundary conditions

$$u(0,t) = 0 \qquad\qquad u(L,t) = 0 \tag{A.2}$$

for all $t > 0$, and the initial condition

$$u(x,0) = f(x) \tag{A.3}$$

Because of (A.2), f has to satisfy $f(0) = f(L) = 0$.

The most common method to solve this equation is by employing separation of variables:

$$u(x,t) = F(x)G(t) \tag{A.4}$$

Substituting (A.4) into (A.1) gives

$$\frac{\dot{G}}{c^2 G} = \frac{F''}{F} = -p^2 \tag{A.5}$$

which yields two ordinary differential equations:

$$F'' + p^2 F = 0 \tag{A.6a}$$
$$\dot{G} + c^2 p^2 \, G = 0 \tag{A.6b}$$

Equation (A.6a) leads to the solution family:

$$F(x) = A\cos px + B\sin px \tag{A.7}$$

The unique solution is found by applying the boundary conditions (A.2):

$$F_n(x) = \sin\frac{n\pi x}{L} \qquad\qquad n = 1, 2, \ldots \tag{A.8}$$

The temporal component, $G(t)$, is solved as

$$\dot{G} + \lambda_n^2 \, G = 0 \qquad\qquad \lambda_n = \frac{cn\pi}{L} \tag{A.9}$$

which leads to the general solution

$$G_n(t) = B_n e^{-\lambda_n^2 \, t} \qquad\qquad n = 1, 2, \ldots \tag{A.10}$$

where B_n is a constant.

Using (A.8) and (A.10), solutions to the heat equations can be written as

$$u_n(x,t) = F_n(x)G_n(t) = B_n \, \sin\frac{n\pi x}{L} \, e^{-\lambda_n^2 \, t} \qquad\qquad n = 1, 2, \ldots \tag{A.11}$$

$u_n(x,t)$ are called *eigenfunctions* of the heat equation corresponding to the eigenvalues $\lambda_n = \frac{cn\pi}{L}$. These functions represent individual modulations of the entire solution, which is obtained by

$$u(x,t) = \sum_{n=1}^{\infty} u_n(x,t) = \sum_{n=1}^{\infty} B_n \, \sin\frac{n\pi x}{L} \, e^{-\lambda_n^2 \, t} \qquad\qquad \lambda_n = \frac{cn\pi}{L} \tag{A.12}$$

From the initial condition, $u(x,0) = f(x)$, we obtain

$$B_n = \frac{2}{L} \int_0^L f(x) \sin\frac{n\pi x}{L} \, dx \qquad\qquad n = 1, 2, \ldots \tag{A.13}$$

The nonhomogeneous heat equation has the following form:

$$u_t - c^2 u_{xx} = q \tag{A.14}$$

where q represents uniform volumetric heat generation rate. Equation (3.b) has this form.

The solution to the nonhomogeneous form is found by using the following substitution:

$$u(x,t) = v(x,t) + w(x) \tag{A.15}$$

subject to the boundary conditions $v(0,t) = v(L,t) = 0$, and the initial condition
$v(x,0) = f(x) - w(x)$. $w(x)$ is determined by enforcing that $v(x,t)$ satisfy the homogenous part, that is,

$$v_t - c^2 v_{xx} = 0 \tag{A.16}$$

Substituting (A.15) into (A.14) yields

$$v_t - c^2(v_{xx} + w_{xx}) = \underbrace{v_t - c^2 v_{xx}}_{0} - c^2 w_{xx} = q \tag{A.17}$$

which leads to

$$w_{xx} = -\frac{q}{c^2} \tag{A.18a}$$

$$w(x) = \frac{-q}{2c^2}\, x^2 + ax + b \tag{A.18b}$$

subject to $w(0) = w(L) = 0$, because of the boundary conditions, which yields

$$w(x) = -\frac{q}{2c^2}\,(x^2 + Lx) \tag{A.19}$$